Tampere University

Pyry Lampinen

ANALYSIS OF GLASS TEMPERING FURNACE DATA

Faculty of Engineering and Natural Sciences
Master of Science Thesis
January 2020

ABSTRACT

Pyry Lampinen: Analysis of Glass Tempering Furnace Data
Master of Science Thesis
Tampere University
Degree Programme in Automation Technology
January 2020

The data of a glass tempering furnace is analyzed in this work. In this work is created an algorithm for the data to be interpolated and transformed from stationary measurements into the moving glass frame in order to create comprehensive data of temperatures that the glass has "seen" during the heating of the glass.

The transformed data is then analyzed with principal component analysis and it was found out that PCA was able to compress data into a few principal component scores. The principal component scores form a single tempering instance contained a clear spatial structure that correlated with the layout of the tempered glass panes.

Finally, an automated method of separating deviant tempering instances using the principal component scores was developed. A correlation between deviant tempering instances and idle time of the tempering furnace before the tempering process was found out.

Keywords: glass, tempering, PCA, principal component analysis, coordinate transformation

TIIVISTELMÄ

Pyry Lampinen: Lasinkarkaisu-uunin datan analysointi
Diplomityö
Tampereen yliopisto
Automaatiotekniikan koulutusohjelma
Tammikuu 2020

Tässä työssä analysoitiin lasinkarkaisu-uunin tuottamaa dataa. Työssä kehitettiin algoritmi, jolla data on interpoloitu ja stationaariset mittaukset uunista on muunnettu liikkuvan lasin koordinaatistoon, jotta saadaan kattava kuva lämpötiloista, joita kunkin lasipisteen kohdalla uunista on mitattu karkaisun aikana.

Muunnettua dataa on tämän jälkeen analysoitu käyttämällä pääkomponenttianalyysiä, jonka tuloksena havaittiin, että data voidaan pakata käyttämällä vain muutamaa pääkomponentin pistettä (*engl. score*). Pääkomponenttianalyysin pisteet yhdestä lasinkarkaisusta tuottivat dataa, jolla oli selkeä spatiaalinen rakenne, joka korreloi karkaistujen lasien lastausmuodon kanssa.

Lopuksi työssä kehitettiin automaattinen menetelmä erottelemaan poikkeavat karkaisut pääkomponenttianalyysin pisteiden avulla. Testisarjasta löydettiin tämän avulla poikkeavia lastauksia, joiden poikkeama vaikutti olevan yhteydessä karkaisu-uunin odotusaikaan ennen karkaisua.

Avainsanat: lasi, karkaisu, PCA, pääkomponenttianalyysi, koordinaattimuunnos

PREFACE

I wish to express great gratitude to my supervisor, Professor Risto Ritala, for introducing me to the topic and for the excellent help and guidance during the process. I want to thank my colleagues at Glaston Finland Oy and the Department of Automation Technology and Mechanical Engineering as well for their help and insights during the work. Glaston Finland Oy is also acknowledged for the topic and the financial support for the thesis.

Finally, I would like to thank my family for their support and encouragement.

Tampere, 31st January 2020

Pyry Lampinen

CONTENTS

LIST OF FIGURES

LIST OF TABLES

LIST OF SYMBOLS AND ABBREVIATIONS

A	Matrix of principal component loadings on its columns
a_i	Value of i^{th} barycentric coordinate
α_i	i^{th} principal component loading
$\mathcal{C}_i$	Principal component's contribution to the inertia
csv	comma separated file
CVD	Chemical vapour deposition
Δ	Diagonal matrix of singular values
dF	Deviation from $\overline{Fm}$
DS_m	detection score of m^{th} measurement
E	Sum of squares of difference
η	Efficiency of the quenching fan
F	Matrix of principal component scores
f_i	i^{th} principal component score
$F^{[k]}$	F-matrix containing k score elements
$\overline{Fm}$	Average PCA scores
f_{sup}	Supplementary principal component scores
furnace_reading	3-dimensional matrix containing data in stationary coordinates in Algorithm 1
glass_frame	3-dimensional matrix containing data in moving frame in Algorithm 1

H	Heaviside function
$\mathcal{I}$	Trace of the covariance matrix K_{SS}
I_N	Identity matrix with dimensions N x N
json	JavaScript Object Notation
K	number of attributes in S in Section 4.1
k	Number of principal components used
κ	Condition number of a matrix
K_{SS}	Covariance matrix of S
$\mathcal{L}$	Lagrangian function
λ	Eigenvalue
Low e	Low emissivity glass or coating
m	meter
MSVD	Magnetron sputtering vapor deposition
μ	Mean of data set
N	number of samples in S in Section 4.1
n	Number of vertices
P_{fin}	Quenching fan power
PCA	Principal component analysis
Q	Normalized eigenvectors of $S^T S$
$Q^{[k]}$	Q-matrix containing k loadings
r	index of tempering instance
R_S	Correlation matrix os S
s	Data sample
S	Data matrix

$\hat{S}$	Data approximated with part of the principal component scores
σ	Standard deviation of data set
σ_m	Standard deviation of Principal component scores
$\overline{s_m}$	the sample mean over X, Y and r
S_n	Normalized matrix of S
SND	Standard normal deviate
SND_m	SND values summed over X, and Y
SND_s	Standard normal deviation of the sample s
S_{std}	Standard deviation of the columns of S
s_{sup}	Supplementary data for principal component analysis
SVD	Singular value decomposition
T	Time in furnace frame
t	Absolute time
t0	Time the coordinate entered the furnace in Algorithm 1
TAU	Tampere University
time_end	Total tempering time in Algorithm 1
θ	Angle of the glass coordinates
TUNI	Tampere Universities
$t_{X,Y}$	Time when point (X, Y) entered the furnace
uint	Unsigned integer
$\dot{V}$	Volumetric flow in quenching
X	X-coordinate in glass coordinates
x_{orig}	X-coordinate of moving origin in furnace coordinates
x0	X-coordinate of the glass coordinates' origin in Algorithm 1

x_end	Length of the glass layout in x-direction in Algorithm 1
x_i	Value at i^{th} vertex
x_{interp}	Interpolated value
Y	Y-coordinate in glass coordinates
y_{orig}	Y-coordinate of moving origin in furnace coordinates

1 INTRODUCTION

In this work, the data of the glass tempering furnace is analyzed. Tempered glass is used widely in multiple applications, such as in façades, glass furniture, and car windshields. The tempered glass has to meet several quality requirements, and in many applications, the optical quality has to be good. The process of tempering glass can induce imperfections to near-perfect float glass. The motivation of this study is to analyze the tempering data in order to improve the tempering process and to be able to predict the outcome of the tempering based on the measurements from the process.

The tempering furnace data consists of temperature readings from fixed locations inside the furnace as well as the data containing the power of the heating elements. As the focus of this research is the thermal treatment of the glass panes, the data is not directly usable because the tempered glass panes move back and forth inside the furnace. This problem should be resolved by an algorithm converting the measurements from furnace coordinates into the glass frame. A research objective of this work is to develop this algorithm and analyze the data produced by it. The specifications for the algorithm are that it must convert the data into the glass frame and shift the starting point of time, so zero-point of time is when any given point enters the furnace.

The research question for this study is: can deviant tempering instances be detected by applying principal component analysis (PCA) on this new data? The temperature profile of the glass during the tempering process has a significant impact on the final result of the process. Intuitively this temperature profile is affected by the temperature history that any given point of the glass has seen.

The structure of this work is the following. First, in Chapter 2, the properties of float glass and its tempering process are described. In Chapter 3, the properties of tempered glass are discussed. The theory of principal component analysis is discussed in Chapter 4, and it is followed by the introduction of the data conversion algorithm in Chapter 5. In Chapter 6, the methods of furnace data analysis are discussed, which is followed in Chapter 7 by a case study of a set of tempering instances with similar layouts. Finally, the work is summarized in Chapter 8.

2 FLOAT GLASS TEMPERING

In this Chapter, the properties and the process of producing the float glass are briefly discussed. The discussion is then continued by an explanation of the glass tempering process and principles of a typical glass tempering furnace, which both are explained in more detail.

2.1 Float Glass

From 1920 until 1964, the flat glass was mainly produced by plate and sheet glass processes. The plate glass process produced optically homogeneous glass without imperfections. The downside of this process is that the process required more labor and was capital intensive. The sheet glass process required less capital and suited better for small scale production. The production with sheet glass process was cheaper than with the plate glass process, but the final product contained optical imperfections.

In 1964 Pilkington Brothers Ltd introduced the float glass process, which was adopted to plate glass process and later to sheet glass process as well [1]. Float glass is produced by first feeding molten glass from approximately 1200 °C furnace into a tin bed. The glass flows along the tin bed until it is cooled to approximately 600 °C temperature. After the glass has reached that temperature, it can be lifted onto rollers transferring it to an annealing lehr. Finally, in the annealing lehr, the glass is slowly cooled down in order to avoid the formation of internal stresses. Finally, the glass can be cut to desired measurements. The final result is smooth and optically near-perfect glass. The glass is typically cut into so-called jumbo sheets of size 3.21 m x 6 m [2, p. 2].

The use of a molten tin bed solved the problem of keeping the glass flat during the cooling. The glass thickness is controlled by the rate the glass is poured onto the bed and by a specific actuator controlling the glass width and flow rate at the tin bed. A typical molten tin bath can be up to 50 meters long and up to 4 meters wide [3, p. 5].

The float process is based on the difference in the typical soda-lime-silica glass density (2.3 g/cm^3) compared to the density of tin (6.5 g/cm^3) [4, p. 184]. Tin also has suitable material properties for the process. The melting point of pure tin is at 231.93 °C, and it has a boiling point at 2602 °C. This allows a wide range of temperatures for glass treatment.

The melting of the glass consists of two phases. The first phase is to heat the glass to approximately 1550-1600 °C temperature in order to achieve a homogeneous mix of

the raw material. The molten glass mass is then gradually let to cool to approximately 1200 °C temperature at the pouring end of the furnace. From the end of the furnace, the molten glass is fed onto the tin bed by controlling a specific flow gate called a tweel. A typical float line furnace is approximately 9 m wide and 45 m long and can hold up to 1200 tons of molten glass and operating 24 hours a day for 365 days a year [4, p. 184] [2, p. 2].

Pilkington's invention of the float glass process allowed continuous process glass manufacturing with relatively low labor. Earlier the production of flat optically good glass required grinding and polishing, making the process slow and cumbersome on labor. A modern float line can produce over 500 tons of glass a day.

Presently most of the window glass, mirrors, or anything based on flat glass is produced using the float glass process. Ordinary float glass is soda-lime-silica, which typically consists of 69-74 % silica, 5-14 % lime, 10-16 % soda, and some additives [2, p.4-5]. Another common glass type is borosilicate glass, which has been used, for example, for fire protective glazing. Borosilicate glass consists of 70-87 % silica, 0-8 % of soda, 7-15 % boron-oxide and varying additives [2, p.4-5].

2.1.1 Coated glass

During the float glass process, the glass can be coated online or afterward offline, respectively, to manipulate the glass properties as desired. One of the properties manipulated is the emissivity of the glass. The coating is applied only on one side of the glass.

The emissivity of specific wavelengths can be reduced by adding a thin layer of additives on the glass surface. The reduced emissivity can be a very desirable property of the glass as it helps improving insulation by blocking heat radiation from entering or exiting through a window.

An online method for low emissivity coating (low-e) is chemical vapor deposition (CVD), where the additives are attached to the hot glass. The process bases on exposing glass surface with metal particles such as fluorinated tin dioxide or silver [5]. The result of this process is also called pyrolytic coating.

An offline method for glass coating is magnetron sputtering vacuum deposition (MSVD) in which the additive is attached to the glass surface via sputtering from the anode in a vacuum chamber [6]. The process can be repeated, creating multiple coating layers.

Both of these processes can produce glass with reduced emissivity. Low emissivity glass made with either of the methods can be tempered. However, the low-e coating affects on the heating of the glass as low-e glass absorbs less heat in the furnace, and therefore the coating has to be taken into account while tempering [7, p. 14].

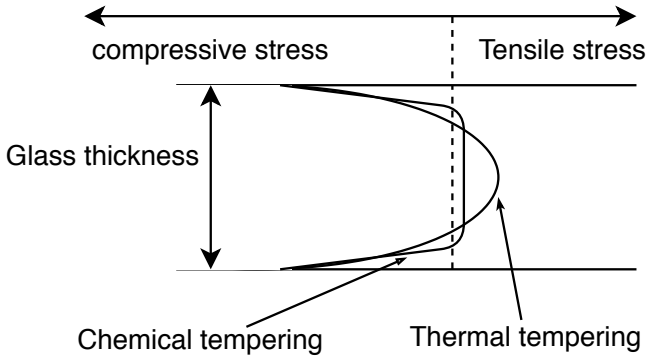

Figure 2.1. *Glass stress profile by thermal and chemical strengthening*

2.1.2 Tempered glass

The physical properties of tempered glass have been modified from those of annealed float glass by generating an internal stress profile. This makes the glass tougher and changes the way the glass shatters from shards to small granular chunks. The physical properties of tempered glass are higher toughness and impact resistance compared to regular, annealed glass. One useful property of tempered glass is that when tempered glass shatters, the result is a pack of tiny fragments that are unlikely to cause injuries. Tempered glass is typically used in applications where shattering glass can produce a danger of injury. Alternatively, tempered glass can be used when higher strength of the glass is demanded. Typical products of tempered glass are rear and side windows of cars, windows, and glass furniture, e.g., glass tables and glass doors.

The tempered glass can be made from annealed glass by treating it thermally or chemically. Thermal tempering begins by heating the glass above its transition point, which is approximately 567 °C depending on the glass properties [7, p. 16]. After the glass has been heated evenly to the desired temperature, it is rapidly cooled down below the transition temperature. The cooling rates of the surface and the inner parts differ, generating residual stress inside the glass. The result is a parabolic stress profile across the glass thickness such that the surface of the glass experiences a tension towards the center of the glass, and the interior of the glass experiences an opposite force.

The chemical glass strengthening is a process that bases on an ion exchange on the glass surface. Smaller sodium ions are exchanged by 30 % larger potassium ions [2, p. 12]. This creates a thin layer of compression on the glass surface. The depth of the compression zone depends on the treatment time. Usually, this process is used when the thermal tempering process is not suitable for the object. Unlike the thermally tempered glass, after chemical strengthening, the glass can still be cut or drilled.

Thermal and chemical strengthening produces different stress profiles in the glass, see Figure 2.1. The chemical strengthening produces a thin compression layer, whereas the thermal tempering produces a parabolic stress profile. The thermal tempering is in focus of this work, and it is discussed more in later Chapters.

2.2 Glass tempering furnace

Glass is thermally tempered in a specific furnace, capable of all the required process stages. A typical glass tempering furnace consists of four main sections: loading table, furnace, quenching section, and unloading table. The glass travels through the sections on rollers, which are driven independently at each section. The rollers are made of steel and are coated with aramid fiber or plastic. The exception is the uncoated ceramic rollers in the heating furnace.

2.2.1 Loading table

The loading table consists of the main rollers and additional rollers that are lifted to support glass and allow its placement on the main rollers. The operator and the control panel are also typically next to the loading table. Typically, there are also rollers on the side of the loading table. These rollers are to assist handling larger glass planes as those can be rolled onto the table.

From the loading table, glass panes are transferred to the furnace. Before entering the furnace, the layout of glass panes is measured optically. The measurement ensures that the subsequent operations know the length of the loading and can process the loading accordingly.

2.2.2 Heating furnace

The Heating furnace is insulated and has doors on both ends for the glass to enter and exit. The furnace is preheated to a specific glass-type dependent temperature. The glass is heated with radiative heat transfer from the heating elements, with forced convection from pressurized hot air and with conduction from the rollers.

The heating elements are located both above and below. The heating elements above the glass are typically arranged in an uneven array where resistors are orientated in the running direction. This allows higher resolution in the cross direction of the furnace. An example layout of the heating elements is illustrated in Figure 2.2.

Below the furnace, there are similarly resistors as above. However, the resistors below are orientated in the cross direction. This layout is illustrated in Figure 2.3. Different orientation is chosen because of the rollers in the oven. The rollers mostly block the direct radiation of the heating elements under the rollers. This leads to indirect heating of the glass as the resistor radiate heat to the rollers, and then the rollers radiate heat to the glass. As a small section of the glass is in contact with the rollers, the rollers transfer heat through conduction as well. The heating elements under the rollers are protected from shattered glass by a metal sheet.

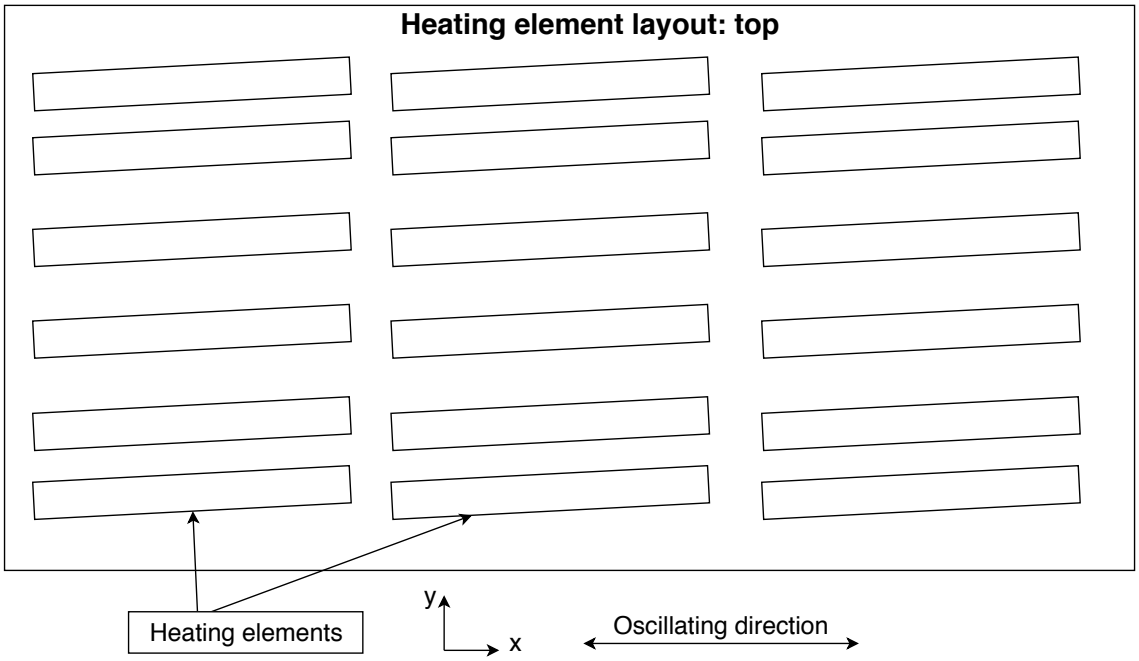

Figure 2.2. *Example layout of the heating elements at the top*

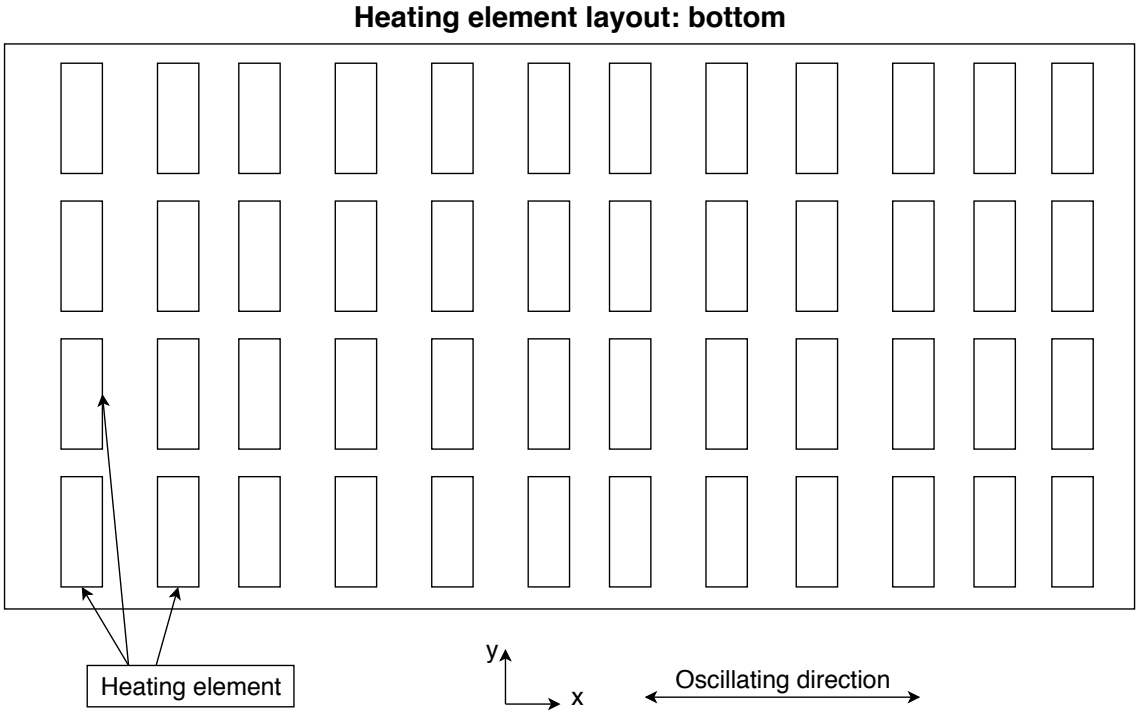

Figure 2.3. *Example layout of the heating elements at the bottom*

The heating element itself consists of a resistor, a convective pipe, and a metal casing. The heating elements have holes on top, allowing the convection air to pass through. There is a thermocouple inside each heating element at the top and typically one thermocouple between longitudinal pair of heating elements at the bottom. These measure the temperatures inside the furnace for control. However, the thermocouples do not detect substantial changes in the furnace temperature fast as they are in a metal casing. This is

a designed feature as it reduces the disturbance by the colder glass in the temperature readings.

During the heating, glass must move inside the furnace to heat up evenly. Furthermore, the glass starts to creep downwards at the points not supported by the rollers when it heats up above the transition temperature. This is called an edge kink, and it can be detected after the tempering process. In order to avoid these issues, the glass can either oscillate in the furnace or continuously move in one direction. The tempering furnace of the latter type is called a continuous tempering furnace. The continuous process is suitable for serial production with similar products. The continuous furnace must be longer than the oscillating furnace or it may consist of multiple furnaces in series. The oscillating furnace is smaller and can adapt to smaller batches and various types of products. Oscillating furnace's main advantage is that its costs are lower due to a smaller size. In the oscillating furnace, the glass oscillates across the heating section during the heating, as illustrated in Figure 2.4.

The forced convection is applied for increased heat transfer into the glass. This is especially important when tempering low-e glass, reflecting up to 90 % of the heat radiation [3, p. 20]. For even heating of the glass, the forced convection is used above, where the glass has been coated. The convection is created with convection blowers on top of the furnace. Alternatively, it can be created by blown convection air via nozzles through the heating elements.

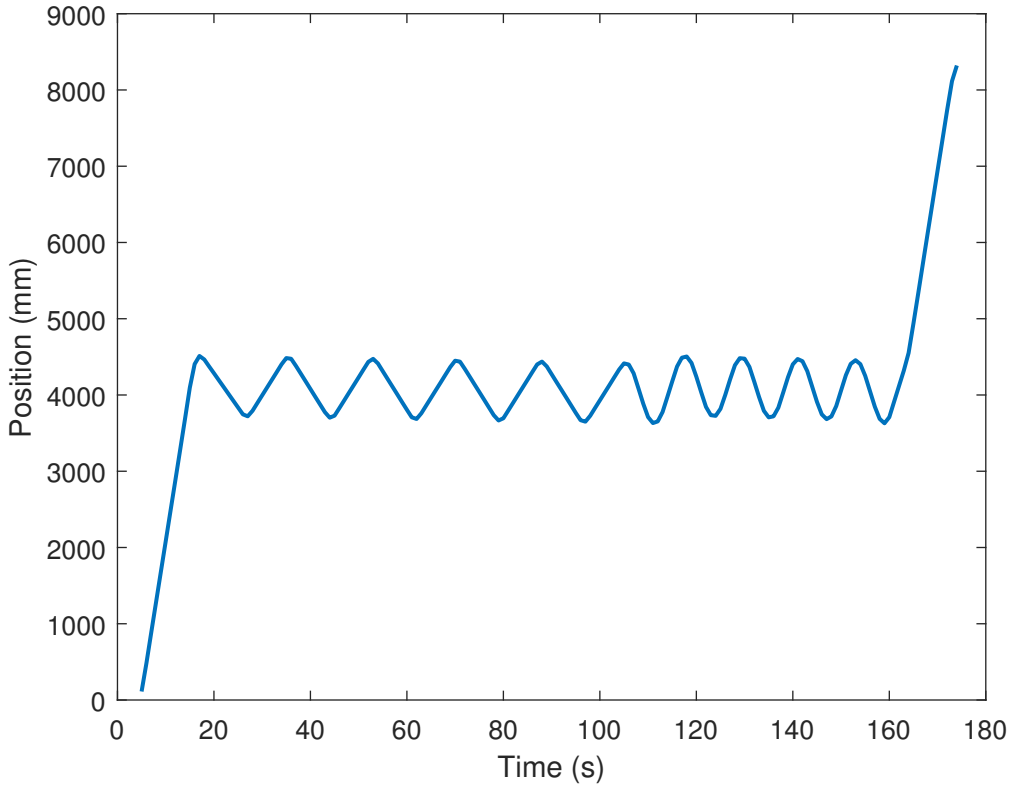

Figure 2.4. *Position curve of the front edge of the glass in the furnace during the heating*

The key issues during the heating are consistent temperature profile across the glass planes, desired temperature, and controlled heating. The latter refers to such heating that the glass does not shatter during it. Thicker glass planes can break due to temperature shock at the early stages of the heating process. Typically, this problem is mitigated by lowering the temperature at the initial part of the heating. In order to increase productivity, the heating time of tempered glass is minimized by using high enough temperatures.

2.2.3 Cooling section

After the glass is heated to the desired temperature, it is transferred to the cooling section. During the transfer between the heating and cooling sections, the glass temperature is read by a scanner. The cooling section is where the actual tempering takes place.

In the cooling section, the glass is rapidly cooled down below the transition temperature. This process is called quenching. The purpose of quenching is to create a temperature difference between the glass surfaces and the mid-plane. This creates residual stress inside the glass as it cools down below the transition point. After that, the cooling can be done more slowly in a more efficient manner.

Glass is cooled by fans blowing air on the top and bottom. The air pressures are kept in balance in order to avoid glass lifting from the rollers. This is done by adding flow guards at the top of the glass between the top nozzle boxes directing the flow after it has reached the glass to mirror the effect of rollers. In some furnaces, the cooling section can accommodate a boost system consisting of high-pressure air jets. These assist the fans and allow glasses down to 3 mm thickness being tempered. The energy consumption of the furnace can be balanced by storing the pressurized air into a pressure vessel.

The required overall cooling and the initial cooling rate depend on the glass thickness. For thicker glass panes, the temperature difference between the surfaces and the mid-plane is easier to achieve. However, the glass plane itself stores more energy and therefore needs more time to cool. For thinner glass planes the opposite is true. The amount of fan power needed for cooling 4mm glass compared to 8mm glass can be 42-times greater [3, p. 21]. The required quenching pressure is approximately proportional to the inverse of the third power of thickness [7, p. 45].

The fan power P_{fin} required for quenching is determined by equation

$$P_{fin} = \frac{\Delta p \dot{V}}{\eta}, \tag{2.1}$$

where Δp is the pressure difference, $\dot{V}$ is the volumetric flow and η is the efficiency of the fan [3, p. 99]. The equation holds for moderate pressure differences when the flow is incompressible.

During the quenching, the glass is oscillating in the cooling section for even cooling and to avoid markings from the rollers on the glass. After quenching, typically glass is slowly

cooled down until it reaches temperatures that allow handling of the glass.

2.2.4 Unloading table

Finally, the tempered glass is transferred from the cooling section to the unloading table. When the glass has reached the unloading table, the additional rollers are lifted for easy handling of the glass. After the glass has been convoyed to the unloading table, the operator inspects it visually, and the tempering of the next batch can be started.

2.2.5 Operating the tempering furnace

The furnace is controlled by its operator. The operator decides the layout of the glass planes that are going to the tempering. Then the operator has to choose the heating time and other parameters for the tempering.

Among the parameters that the operator is able to change are the heating time and profile, which controls the temperature set points during the heating across the furnace, offsets of the individual heating elements in the furnace, and a heating and cooling recipe. The recipes are sets of glass-type specific parameters. The choice of the recipe is based on the thickness and type.

The operating panel stores parameter sets for later use and the operator can choose suitable ones from there and customize them if needed. Some typically customized parameters are the heating elements' offsets and conveyor speeds during the tempering. However, the availability of the recipes does not guarantee good tempering results, and a skilled operator can make consistently good glass.

2.3 Glass tempering furnace measurements

This Section focuses more specifically on Glaston glass tempering furnaces. The glass tempering furnace produces a set of data from each cycle of loading, heating, quenching, and unloading. Important measurements from the process are the temperatures inside the furnace, powers of the heating elements, and the glass temperature before quenching, read by a thermal scanner, which is typically located under the rollers. The data given by the operator is saved along with some furnace specific parameters.

This data is essential for many purposes, such as finding a faulty component, determining causes of anomalies in the tempering process, and evaluating the results of the process. This data allows analysis of the process and its further development.

The furnace temperature is monitored from each heater box above the rollers and between each heater pair below the rollers. The temperature is measured by a thermocouple, and the data of readings from the top and the bottom is saved into a database at a

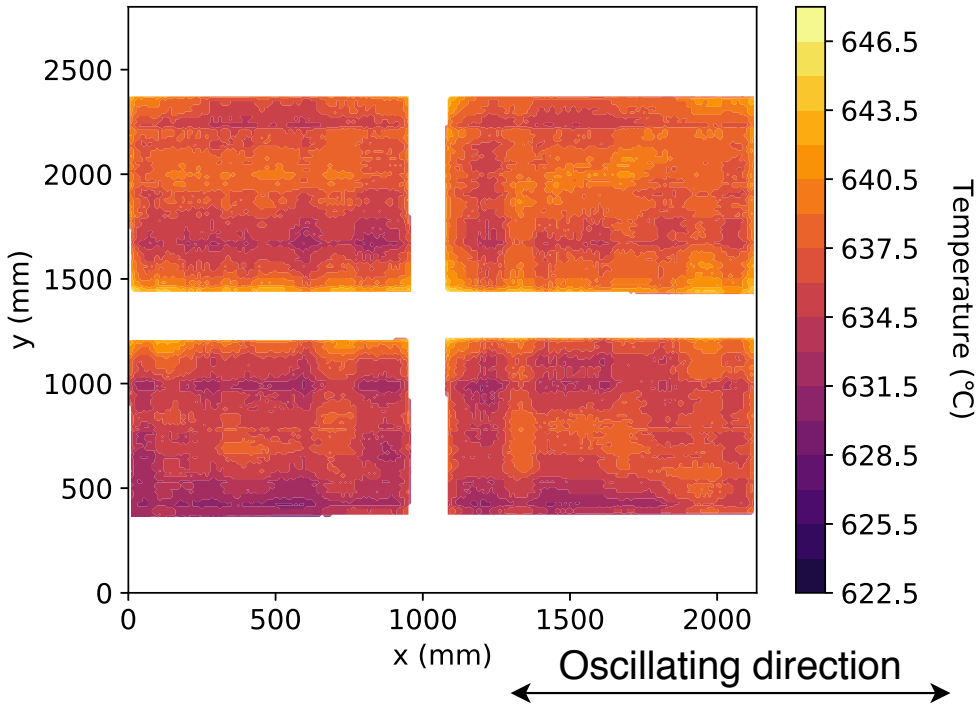

Figure 2.5. *An example scanner image of the glass temperature after the heating*

given sampling rate. The thermocouples have a rather slow response to the temperature changes due to their location inside the heater casing.

During the transfer from the loading table to the furnace, the load length of the glass is measured with an optical gate. This measurement is used to calculate the back-and-forth motion in the furnace. The motion is calculated with a set of desired speeds that the glass should move during different phases of the heating. Typically, the speed is lower during the first stroke in the furnace, and then the speed is increased. This helps to mitigate issues caused by the creeping of the glass as it heats up above the transition temperature.

The position of the glass is currently not logged onto a data file on all tempering furnaces. However, it is possible to replicate the algorithm calculating the speed during the heating as the target speeds can be read from the saved data.

Figure 2.5 shows an example image produced by the data from the temperature scanner. The scanner measures the glass via a mirror under the rollers. The quality of the scanner image can be deteriorated by dust or glass shards on the mirror. On some older glass tempering furnaces, the temperature scanner has been mounted above the rollers. However, a scanner above, i.e., on the low-e side, is not suitable to measure low-e glass's temperature because the lower emissivity results in a false reading. From the bottom side, the temperature of the low-e glass can be read.

3 PROPERTIES AND QUALITY OF TEMPERED GLASS

The annealed float glass has a flat surface and optically excellent properties. However, temperatures and the handling of the glass during the tempering process can degrade these properties. In this Chapter, the changes in the glass during the tempering are discussed.

Quality requirements of tempered glass vary depending on the application. For example, architectural glass and automotive safety glass can have quite different requirements. The quality of tempered glass can be divided into two main categories of interest: optical quality and mechanical quality, each with related standards. The quality of the glass relates to the standards it needs to fulfill. For example, an optical lens can have much tighter tolerances for optical properties than a heat-treated oven window.

3.1 Residual stresses

The residual stresses develop as air jets cool the hot glass rapidly. At first, the glass begins to contract. This is followed by the stiffening of the glass surface as it cools below the transition temperature. The still-hot interior of the glass is contracting because of the contracted surface and the decreasing temperature until it also reaches the transition temperature. Even more stress is generated into the glass because the stiff surface layer starts to resist the interior of the glass contracting anymore. The process of residual stress development is explained by Rantala in [3, p. 16]. Barr [7, p. 22] explains that also the glass interior resists the contraction of the surface at the early stages of the cooling affecting the stress profile. The annealed glass has typically around 2 MPa surface compression, for heat strengthened glass the surface compression is typically 40-60 MPa, and for tempered glass approximately 80-100 MPa [3][8].

The residual stress profiles are illustrated in Figure 3.1, where the surfaces have compressive stress, and the mid-plane of the glass has tension. The tension and compression areas under the curve must be equal due to the equilibrium of forces. The compression is approximate twice the tension in the center [7, p. 30].

These stresses vary along the glass plane corresponding to the differences in the heating and cooling of the glass. The differences in the temperature profile of the glass result differences in residual stress of the glass and can cause other quality problems to the

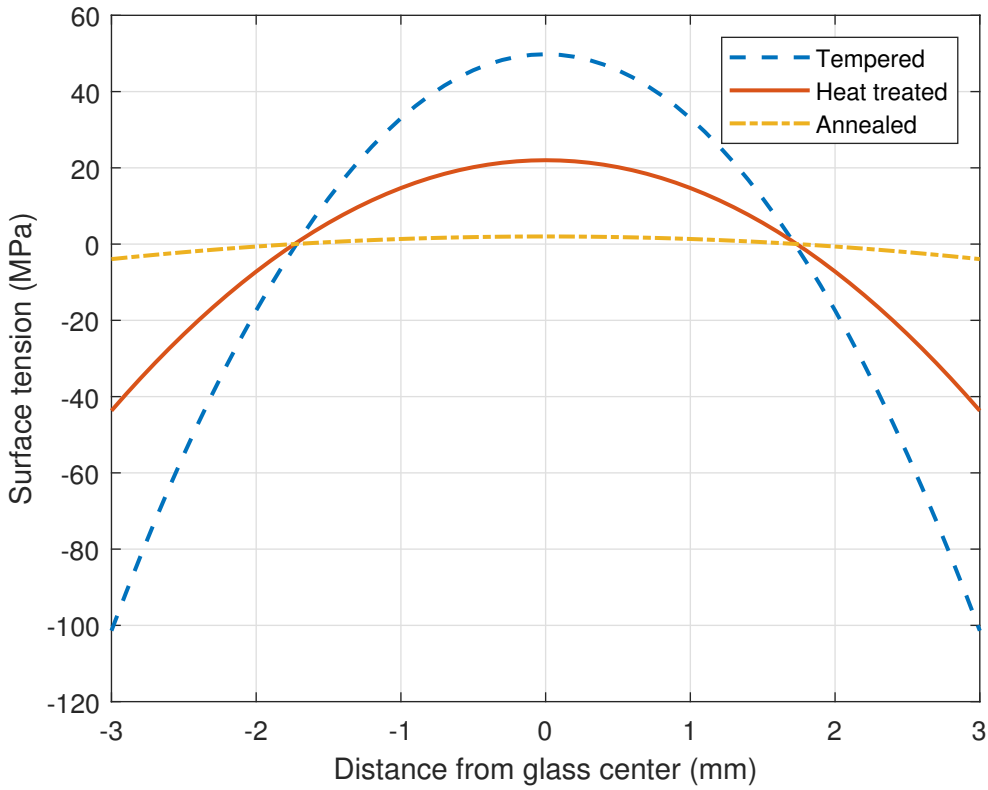

Figure 3.1. *Typical tension profiles of the glass*

glass.

3.2 Anisotropy of tempered glass

The anisotropy of glass manifests itself as birefringence, i.e., the glass reflects optical waves of different polarization differently [9]. The term anisotropy itself refers to the non-uniform distribution of properties among the glass pane. The angle of birefringence depends on the residual stresses in the glass [10] [11].

The residual stresses change the optical properties of the glass. As the residual stresses are necessary for glass tempering, the transition to birefringent material is inevitable. Only the uniformity of the stress pattern on the pane can be controlled.

The differences in anisotropy can be seen as lines or circular patterns on the glass at some conditions. The patterns are visible when polarized light refracts from the glass. Typical sources of the polarized light can be blue sky and reflections from other glass or water.

3.3 Mechanical quality

The mechanical quality of the glass can be measured in several ways as many issues can become a problem during the tempering. The most apparent mechanical problem with the glass tempering is glass shattering during the tempering process. This can be caused by inappropriate heating or some imperfections on the glass itself. There are two main reasons for the glass shattering. During the heating, the glass can shatter due to thermal shock. This can be avoided by lowering the temperature during the initial heating. Another critical phase is quenching. Typically, the glass shatters during the quenching if it is initially too cold. This can be avoided by heating the glass more.

One of the mechanical defects is the bending of the glass. This happens when the glass is heated unevenly. During the heating, glass expands. If the temperatures on the sides differ, the glass pane bows on the hotter side. This is because the hotter side of the glass shrinks more during quenching than the other side, causing the bow on the hotter side. Bending can happen locally, or the entire glass can bend.

The glass can bend to a stable or unstable shape during the tempering. A stable shape cannot be flipped. The glass that is overheated from the edges can turn into a saddle shape as the edges will expand more than the middle section. This shape is typical for thinner glasses and an unstable shape, and the glass can be flipped to be saddle-shaped in the opposite direction as well.

The glass reaches near plastic properties when heated above the transition temperature. This causes the glass to creep downwards during the heating. This can be a problem at the edges of the glass as they are unsupported while moving from a roller to another. This defect, called edge kink, means that the glass is bent from the front and rear edges. The edge kink is illustrated in Figure 3.2. In order to make the support from rollers more uniform, the glass is oscillating in the furnace.

As the glass oscillates to newly heated rollers, the front and rear edges of the glass may become overheated and start to creep downwards, which results in chipping. This problem is typically mitigated by reducing the temperature at the edges of the furnace by changing the temperature offsets of the heating elements. The creeping is also the main cause of the wavy shape of the glass as it adapts to the support of rollers. This defect is called roller waves. If the rollers are not prcisely on the same level, or some of the rollers are slightly eccentric, the glass will adapt to that shape. The roller waves are themselves not a significant issue mechanically as the creeping is rather small, but it is easily visible

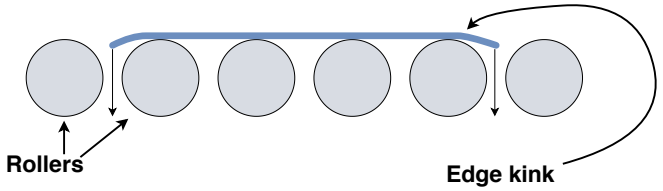

Figure 3.2. *Edge kink of the glass in the furnace.*

optically [7].

Aronen and Karvinen [12] have summarized that the glass is a viscoelastic material and the viscous effect increases when the temperature exceeds the transition point, causing edge bending and roller waves. The waves can also be caused by the creeping edges, which affect across the glass moving direction. The mechanical behavior of the glass during tempering is also widely discussed by Aronen in [8].

3.4 Optical quality

The optical quality refers to the defects that distort the reflection or visibility through the glass or other optical imperfections on the glass. Usually, the optical quality of the glass affects more to the reflections from the glass.

The changes in residual stresses inside the glass plane cause the glass to block certain orientations of polarized light. This can be clearly seen when observing polarized light passed through the glass with a polarizing filter. The cause of this effect is briefly explained in Section 3.2.

The stress differences and uneven heating can be caused by the ceramic rollers as the glass changes direction during oscillation. This conducts more heat locally to the area above the rollers. The markings produced this way are called oscillating lines. Oscillation lines and stress patterns from quenching are dependent on the tempering equipment and process parameters such as heating time, temperature, and speed of the conveyors.

Another issue causing stress differences is the aramid fiber spooled onto the rollers at the cooling section. These cords conduct little heat to the glass but obstruct the airflow, hence reduce quenching directly above them.

Mechanical defects can also cause optical defects. The bowed glass or glass with noticeable roller waves distorts the reflection from it. Another issue caused by mechanical defects is the so-called white haze. This results from the uneven pressure of the rollers as the glass arches to either side. If the glass bows and the center of the glass bows downwards, the rollers can cause markings on the glass.

The optical quality and its requirements depend on the application. For example, for a large façade project, the minimal differences in anisotropy are favorable. If the annealed glass is not an option, the uniform anisotropy pattern and the same alignment of the panes are critical [9]. Using a mock-up on-site glass pane test installation, the quality of the glass can be verified according to the real conditions [9].

3.5 Avoiding quality defects

The common cause for many of the defects is unsuitable heating. Some defects, such as oscillation lines and markings from the aramid fiber occur always with typical tempering

furnace, but they can be reduced with appropriate tempering parameters. The monitoring of the temperature inside the furnace and an accurate estimate of the glass temperature can help in determining the causes of quality problems.

There are ways to mitigate these problems with tempering settings, but the changes in anisotropy cannot be avoided entirely. Ways to reduce stress differences in the glass pane are changes in the heating or quenching process [13]. For example, lowering the furnace temperature and increasing the heating time helps to ensure even heating of the glass. Another option is reducing the loading speed during the quenching to cool the glass before the first change of direction. However, typically these changes reduce the production capacity and overall efficiency. By keeping the temperature of the glass lower, some of the defects, such as roller waves and edge kinks can be reduced. The downside of this is that quenching colder glass increases the risk of breaking the glass during quenching [7, p. 38].

Another important issue is keeping the glass flat during the tempering. This is especially difficult for large glass panes [3, p. 16]. The glass can be kept flat with suitable parameters and by paying attention on keeping the heating even on both sides of the glass [3, p. 16].

4 PRINCIPAL COMPONENT ANALYSIS

Principal component analysis (PCA) is a statistical method of interpreting data where the data with correlated values is transformed into a set of linearly uncorrelated values. The method is originally presented by Pearson in [14]. PCA has four primary purposes:

1. extract the essential information,
2. reduce the size of the data,
3. simplify the data and
4. enable a structural analysis of the measurements [15].

In other words, the analysis reduces the dimensionality of the data set. This is especially useful if the original data contains interrelated variables. PCA yields the new data with most of the variation of the original data in a more compact form [16].

4.1 Definition of principal components

The basis for the principal component analysis is a data matrix S in which the row index numbers the attributes (totally K) measured, and the column index numbers the samples (totally N). Typically, the data is also centered by removing the column-wise mean. This matrix is denoted by S_c and is called a centered data matrix.

When the PCA is calculated for a single tempering instance, the data has to be ordered in a matrix containing readings from the same glass coordinates' time instances in the same column. In other words, the data has to be ordered into a list of time series. In order to reconstruct the data onto its correct X-, and Y- positions, the order has to be known. The PCA itself can be done without considering the physical locations of the time series.

The definition of principal components is a set of orthogonal column vectors $\alpha_i, i \in [1, K]$. The α-vectors are chosen such that their scores, defined as

$$f_i = S_c \alpha_i, \tag{4.1}$$

are uncorrelated, where f_i is a column vector containing i$^{\text{th}}$ principal component scores of the rows of S_c. The requirement of uncorrelatedness results in the orthogonality of

α-vectors and the vectors are ordered according to their variances so that the product $S_c\alpha_1$ has a maximum variance.

The α-vectors are called here factor loadings, but depending on the source, they can be called as well as principal PC loadings, coefficients, weights, and eigenvectors.

The product of S_c and matrix A containing factor loadings on its columns results in an N by K matrix F containing factor scores of every principal component

$$F = S_c A. \tag{4.2}$$

If the principal components have been calculated from data set S_c, the set is called active data. However, the factor scores can also be calculated for new data if the number of samples (N) is the same. Typically, the new data is called supplementary or illustrative data, and it is denoted as:

$$f_{sup} = s_{sup} A, \tag{4.3}$$

where s_{sup} is a row vector with K elements.

The covariance matrix of S_c and S is K_{SS}. It can be formed by the cross product of $S_c^T S_c$

$$K_{SS} = \frac{S_c^T S_c}{N-1}, \tag{4.4}$$

which results in an unbiased estimate of the sample covariance. If the data in different columns represent different physical quantities, it may be useful to normalize the data first. The normalization of the data is done by dividing elementwise the columns of centered data matrix by the column's standard deviation

$$S_n = (\mathbb{1} S_{std}^{-1}) \circ S_c, \tag{4.5}$$

where S_{std} is an N by 1 vector containing column-wise standard deviations of S, and $\mathbb{1}$ a 1 by K vector containing ones. The correlation matrix is calculated similarly as in Equation 4.4 by using the normalized data matrix

$$R_S = \frac{S_n^T S_n}{N-1}. \tag{4.6}$$

The principal components can be solved for either the correlation matrix or covariance matrix yielding different results. The decision between the two matrices depends on whether the samples are equally interesting or the samples with higher variance are more interesting. The differences of using either of the matrices is discussed more in [16].

The variance of S projected onto i^{th} principal component of S is

$$\mathsf{E}((f_i - \mu_{f_i})^T (f_i - \mu_{f_i})) = \mathsf{E}((S_c\alpha_i)^T (S_c\alpha_i)) = \mathsf{E}((\alpha_i^T S_c^T)(S_c\alpha_i)) \tag{4.7}$$

where μ_{f_i} is the mean of the i[th] principal component score and μ_{S_c} is the column-wise mean of the data matrix S. This can be calculated by replacing the right-hand side expectation by the covariance matrix, and the vector multiplication of the stationary α_i can be moved outside of the expectation

$$\mathsf{E}((f_i - \mu_{f_i})^T(f_i - \mu_{f_i})) = \alpha_i^T K_{SS} \alpha_i. \tag{4.8}$$

If the principal components are ordered in descending order, the first principal component produces the maximum variance, which can be written using Equation 4.7

$$\begin{aligned} \alpha_1 = \underset{\alpha}{\text{maximize}} \quad & \alpha^T K_{SS} \alpha \\ \text{subject to} \quad & \alpha^T \alpha = 1, \end{aligned} \tag{4.9}$$

where in order to keep α finite, it is bounded to have the sum of squared elements equal to 1. The constrained optimization problem can be solved with the Lagrange multiplier. The first step is to form the Lagrangian equation which becomes

$$\mathcal{L}(\alpha_1, \lambda) = \alpha_1^T K_{SS} \alpha_1 - \lambda(\alpha_1^T \alpha_1 - 1), \tag{4.10}$$

where λ is the Lagrange multiplier. The function reaches its maximum when

$$\nabla \mathcal{L}(\alpha_1, \lambda) = 0. \tag{4.11}$$

Differentiating Equation 4.10 in respect to α results

$$K_{SS} \alpha_1 - \lambda \alpha_1 = 0. \tag{4.12}$$

This can be reordered by using identity matrix I_N with dimensions $(N \times N)$. The result

$$(K_{SS} - \lambda I_N)\alpha_1 = 0 \tag{4.13}$$

is the equation of the eigenvalue and eigenvector. This applies to all principal components. The eigenvectors of the symmetric matrix satisfy the requirement of orthogonality. λ is an eigenvalue of K_{SS}, and α is its corresponding eigenvector. The choice of eigenvector and eigenvalue -pair can be derived for the highest variance from the original goal of Equation 4.9 and Equation 4.12 by multiplying it by α^T from the left. This results in an equation

$$\alpha^T K_{SS} \alpha = \alpha^T \lambda \alpha \tag{4.14}$$

which can be rewritten as

$$\mathrm{E}((f-\mu_f)^T(f-\mu_f)) = \alpha^T\alpha\lambda = \lambda. \tag{4.15}$$

The eigenvalues of the covariance matrix are the variances of the principal component scores. The first principal component is the eigenvector corresponding to the largest eigenvalue, and the rest of the principal components are defined similarly by descending order of eigenvalues. An uncommon issue that can arise from the previous definition is the case of multiple eigenvalues with the same value. The issue is discussed in [16, p. 27], and here only noted that the data can be represented with all the unique eigenvectors.

The goal of PCA is to find a set of orthogonal principal components of the data which maximize the variance along the component's axis. The solution for this is the eigenvectors of the matrix. The maximum variance is achieved with the eigenvector corresponding to the largest eigenvalue [17, p. 343]. The next component is the eigenvector corresponding to the second largest eigenvalue and the rest can be calculated by the same principle.

PCA for a data set S_c results in a set F containing PC scores $f_m(X, Y, k)$ where X, Y is the position of the measurement in glass coordinates, subscript m is measurement, and k is an index of principal component used.

4.2 Finding principal components with singular value decomposition

The principal components of a data matrix can be calculated directly by using eigenvalues and eigenvectors, or the process can be done by singular value decomposition (SVD). The latter method allows the usage of more efficient methods. It is also numerically more robust than the method using eigenvectors.

The principal components can be calculated directly with SVD

$$S = P\Delta Q^T, \tag{4.16}$$

where P is the matrix of normalized eigenvectors of $S_cS_c^T$, Δ is the diagonal matrix of singular values and Q is the matrix of normalized eigenvectors of $S_c^TS_c$. This can be proven by multiplying the equation from both sides by its transpose:

$$S_cS_c^T = P\Delta Q^TQ\Delta P^T = P\Delta^2P^T \tag{4.17}$$

and then multiplying it from the right with P:

$$S_c S_c^T P = P\Delta^2. \tag{4.18}$$

The same applies to Q,

$$S_c^T S_c = Q\Delta P^T P\Delta Q^T = Q\Delta^2 Q^T \tag{4.19}$$

and multiplying from the right by Q

$$S_c^T S_c Q = Q\Delta^2. \tag{4.20}$$

An interesting result of the right eigenvectors Q is that this can be written with the correlation matrix

$$S_c^T S_c Q = (N-1)K_{SS}Q = Q\Delta^2. \tag{4.21}$$

This shows how the SVD can be used to find the eigenvalues and eigenvectors. The eigenvectors of a matrix are the same regardless of any scalar nonzero multiplier, but the eigenvalues are scaled by the multiplier.

With SVD, the calculation of $S_c^T S_c$ can be avoided and therefore avoid significant rounding errors [17, p. 345]. It has to be noted that eigenvectors are the same, but eigenvalues of the covariance matrix can be obtained from the square of singular values divided by $N-1$.

In order to prove the increased accuracy gain by SVD, the condition number has to be introduced. The condition number is a measure of the matrix condition or how much perturbations affect the computation. For example, for a linear model,

$$\hat{A}\hat{x} = \hat{b}, \tag{4.22}$$

the condition number describes how much the solution of $\hat{x}$ is affected by a perturbation in $\hat{b}$. The condition number is denoted by κ, and for normal matrix such as S_c it can be calculated by

$$\kappa(S_c) = \frac{|\lambda_{max}|}{|\lambda_{min}|}, \tag{4.23}$$

where λ_{max} is the maximal eigenvalue and λ_{min} the minimal eigenvalue of S_c. From

equation 4.23 the condition number of the K_{SS} results

$$\kappa((N-1)S_c^T S_c) = \frac{|(N-1)\lambda^2_{S_c-max}|}{|(N-1)\lambda^2_{S_c-min}|} = \left(\frac{|\lambda_{max}|}{|\lambda_{min}|}\right)^2 = \kappa(S_c)^2. \tag{4.24}$$

The principal component scores F can be calculated with SVD as:

$$F = P\Delta. \tag{4.25}$$

Using Equation 4.16 and knowledge of $QQ^T = I$ due to orthogonality, this can be rewritten as:

$$F = P\Delta Q^T Q = SQ \tag{4.26}$$

4.3 Properties of principal component analysis

The PCA has useful properties in the sense of data analysis. It can be used in dimension reduction. The information held by each principal component can be determined from the components' variances described in Equation 4.15. The data set can be approximated using only part of the principal components. The approximated data is denoted by $\hat{S}$, and it can be calculated by

$$\hat{S} = \sum_{i=1}^{k} f_i \alpha_i \tag{4.27}$$

Where α_i is the i^{th} principal component loading, f_i the corresponding PC scores, and k the number of components used in the estimate. The estimate of S is useful as it contains the data that explains most of the variance of the original data; hence it helps to focus on more essential parts of the data.

The error of the estimate can be evaluated as a sum of squares of the difference

$$E = \left\| S - \hat{S} \right\|^2 = \mathcal{I} - \sum_{i=1}^{k} \Delta^2_{i,i} = \sum_{i>k} \Delta^2_{i,i}, \tag{4.28}$$

where $\mathcal{I}$ is the trace of the covariance matrix K_{SS}, and it equals the sum of squared singular values of the L_{SS} [15]. Another interesting result is the principal component's contribution to the trace $\mathcal{I}$, which can be defined as

$$\mathcal{C}_i = \frac{\Delta_{i,i}}{\mathcal{I}}. \tag{4.29}$$

This could be used as a tool in the selection of the number of principal components used. One method of selecting the number of principal components is to keep components with eigenvalues that are above average [15, p. 441]. More methods of choosing the principal components are discussed in [18].

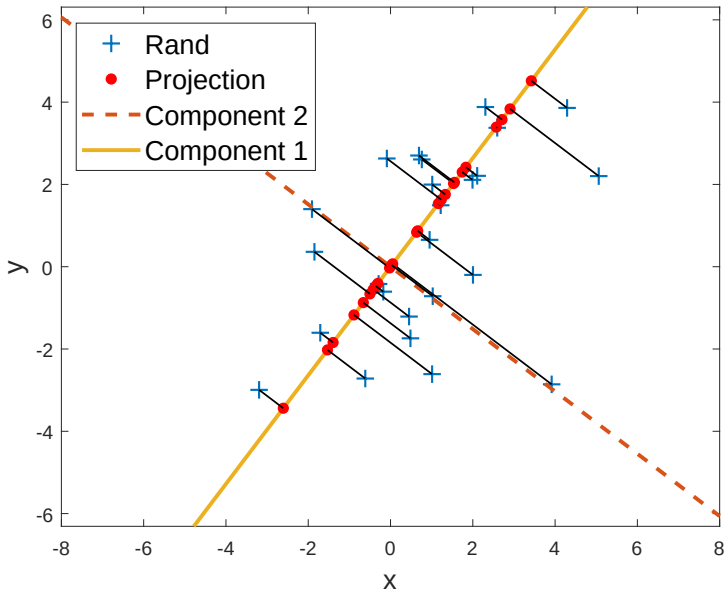

Figure 4.1. *Random bivariate data and its principal components*

4.4 Interpreting principal component analysis

The results of the PCA require interpretation. The information of the PCA is not equally distributed along the principal components. As seen in Section 4.1, the maximum variance of the factor score is on the first principal component, and the variance is descending with the rest of the components. This makes the first component the most important.

In the case of two variables, the PCA can easily be represented geometrically. In Figure 4.1 there are 90 data samples with zero mean covariance of

$$K_{SS} = \begin{bmatrix} 2 & 1.5 \\ 1.5 & 5 \end{bmatrix}, \tag{4.30}$$

resulting

$$\alpha_1 = \begin{bmatrix} 0.6039 \\ 0.7970 \end{bmatrix}, \alpha_2 = \begin{bmatrix} -0.797 \\ 0.6039 \end{bmatrix}, \lambda_1 = 6.2925, \lambda_2 = 2.4254, \tag{4.31}$$

loadings and corresponding eigenvalues, respectively. The axes defined by principal component loading have also been drawn in the figure. The PC scores are simply the data values projected onto both components, as it can be noted from Equation 4.26. The projected values are illustrated in Figure 4.2, where the axis are now the principal components. The principal component analysis rotated the axis by maximizing the data variance along its main axis. On a higher dimension, the principle is the same. The second PC in the example has only one option due to the requirement of orthogonality. At higher dimensions, the remaining components follow the pattern of maximizing variance.

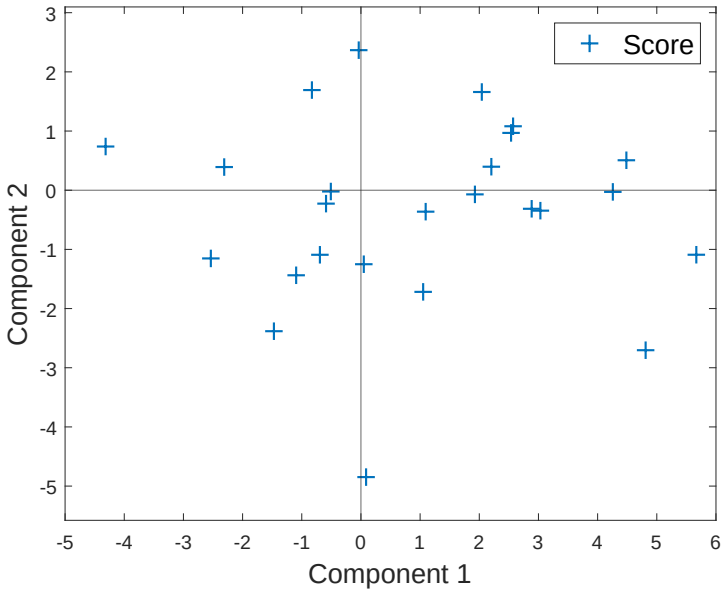

Figure 4.2. *Data shown in coordinates defined by the principal components*

4.5 Statistical analysis

The PCA results in a large amount of data that requires further processing before conclusions can be made. The statistical analysis provides tools to interpret the results of PCA. One useful tool is the *standard normal deviate* (SND). This can be explained as the number of standard deviations between the sample and the data mean, defined as

$$SND_s = \frac{s - \mu}{\sigma} \tag{4.32}$$

where σ is the standard deviation of the data, μ the mean of the data, and s a data sample. The division by standard deviation ensures unit variance, and SND_s describes the significance of the deviation from the mean. SND_s for Gaussian distributed data is in the range -3 to 3 with probability 0.9973. SND reduces the score deviation of samples with high variance. If the deviation from the data mean is of interest, the absolute value of the result can be used. This can be used as a reference value, which is compared to a certain threshold in order to detect abnormal deviation from the mean value.

Standard normal deviate is commonly used in literature. In traffic incident detection the use of SND was discussed by [19], [20], [21]. The SND was used to normalize data and in reporting, if the deviation was larger than a set threshold. Other examples of use cases of standard normal deviate are the studies of earthquake activity by [22], [23].

5 CONVERTING FURNACE MEASUREMENTS TO GLASS FRAME

The measurements from the tempering furnace are taken from fixed positions. The focus of this study is the temperature history of the glass and its impact on the glass. Therefore, transforming the measurements from the coordinates in the furnace to the coordinates of the glass is an appealing approach.

This allows focusing on the temperature development of the glass rather than the furnace. However, the transformation may not be very accurate even if the glass motion and sensor locations are known precisely because the dynamics of the sensor and the furnace may cause delays in the measurements. Furthermore, the temperature readings are measurements of the temperature inside the furnace at a given location, not temperatures of the glass.

The furnace temperatures are measured with thermocouples located at the bottom and the top of the furnace, as described in Section 2.2.2. The readings are written into a csv-file during the heating process at a set frequency. The power of heating elements is recorded as well into a similar file. The measurements have timestamps, which can be used to determine the sampling rate. The amount of data depends on the sampling rate and the duration of the tempering process.

The data received from the tempering process can be divided into two parts.

1. Data stored during the heating
2. Data stored after the heating process.

The data stored during the heating process is the temperature readings and powers of heating elements. After the heating, the glass temperature is measured and stored as well as the tempering parameters. This data is stored in another file and it requires no coordinate transformation. For the coordinate transformation, the knowledge of the length of the glass and the motion of the glass is required.

5.1 Coordinate transformation

The coordinate transformation is based on the knowledge of the object's movement. The simplest case is a plane moving in only one direction. The glass coordinates are de-

noted henceforth with capital letters and furnace coordinates in lower-case letters. The x-coordinate in furnace coordinates can be determined by using the knowledge of the location of the glass coordinates' origin. The coordinate transformation from coordinate X in moving frame to corresponding coordinate x in furnace coordinates is

$$x(t) = X(t) + x_{orig}(t), \tag{5.1}$$

where x is the x-coordinate in furnace coordinates, x_{orig} is the location of the glass origin, t is the time, and X is the x-coordinate in the glass coordinates. The origin of the object can be determined from a position curve, such as seen in Figure 2.4.

The same transformation can be extended to more dimensions. For two-dimensional case the equation extends to

$$\begin{aligned} x(t) &= X(t) + x_{orig}(t) \\ y(t) &= Y(t) + y_{orig}(t) \end{aligned}, \tag{5.2}$$

where y is the y-coordinate in the furnace coordinates, y_{orig} is the location of the glass origin y-coordinate, and Y is the y-coordinate in the glass coordinates. The same principle applies in extending the transformation to more dimensions.

If the glass rotates around the origin, the coordinates are related through:

$$\begin{bmatrix} x(t) \\ y(t) \end{bmatrix} = \begin{bmatrix} \cos(\theta(t)) & -\sin(\theta(t)) \\ \sin(\theta(t)) & \cos(\theta(t)) \end{bmatrix} \begin{bmatrix} X(t) \\ Y(t) \end{bmatrix} + \begin{bmatrix} x_{orig}(t) \\ y_{orig}(t) \end{bmatrix}, \tag{5.3}$$

where θ is the rotation angle of the glass around the origin. Here positive rotation direction is counterclockwise about the origin.

In the case of transforming the temperature readings from the furnace to the glass frame, the transformation of the time was also desired as it enables equal examination of the time series. The time in the glass frame can be imagined beginning as any given point of glass enters into the furnace. This way, the absolute time would be delayed in the glass coordinates along the direction which the glass traverses into the furnace.

The absolute time at a given point could now be determined by the knowledge of the time when the given point enters the furnace. This formalizes into an equation

$$t = t_{X,Y}(X, Y) + T, \tag{5.4}$$

where similarly as on earlier equations capital T is the time in the glass coordinates, but now $t_{X,Y}(X, Y)$ is the absolute time of point X, Y entering into the furnace. This can also be determined from the position curve. This assumes that the point does not re-enter the furnace after it has exited.

5.2 Algorithm for the data conversion to the glass frame

The data from the furnace was given as a combination of a csv-file, (comma separated file), which contained the temperature readings and the heating element control values, and a json-file (JavaScript Object Notation) containing the tempering parameters and the scanner readings.

The purpose of the algorithm is to do the coordinate transformation explained in the previous Section combining the resulting data with the scanner data and other process parameters into a single file for easy handling at the later analysis.

The main algorithm consists of three main sections:

- data initialization,
- data transformation,
- data combination and storage.

These steps are explained in the following subsections.

5.2.1 Data initialization

The measurement data on CSV-files is in a 2-dimensional matrix where readings on each row contain all readings from a given time instance. This data is then read to the working memory into 3-dimensional matrices. The readings are according to their physical locations on the first 2 dimensions, as illustrated in Figure 2.2, and the third dimension contains readings at each time step.

The data forms matrices with dimensions corresponding to the thermocouples or heaters and time steps. The data is then copied to a larger matrix corresponding to the whole furnace dimensions at a higher resolution. This creates a sparse matrix with the measurements.

The empty values are filled by interpolating values in the middle and extrapolating to the edges. There are many ways to interpolate, and interpolation methods chosen here are:

- nearest-neighbor interpolation,
- linear interpolation, and
- spline interpolation.

The first method, nearest-neighbor interpolation, is the simplest. It is based on searching the nearest value and copying it to the point being interpolated. This method can be modified by selecting different distance metrics, such as Manhattan, Euclidean, or Chebychev distance. Another option would be the estimation of the value using multiple

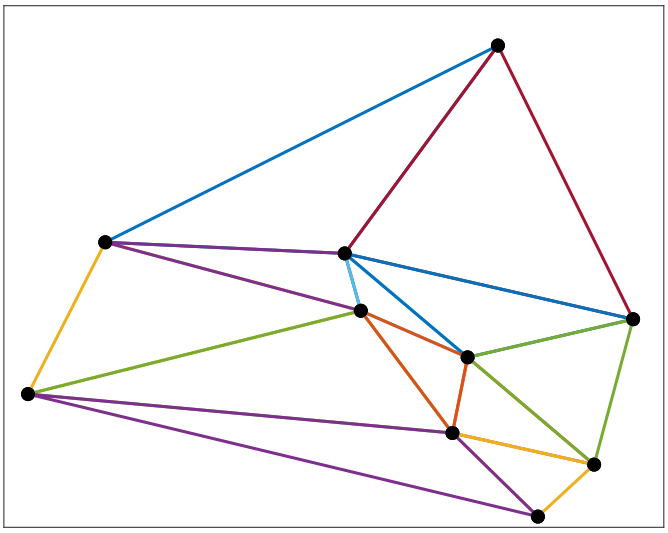

Figure 5.1. *Delaunay triangulation of 10 random data points*

nearest neighbors. One method for solving the nearest neighbors is by creating a k-d tree using the sliding mid-point method described in [24] and finding the nearest match with it.

Nearest neighbor interpolation is easy to implement as it can be applied to the values between the samples as well as outside the samples. It also works well on an uneven grid.

As the thermocouples and heaters are unevenly placed, the interpolation requires a bit more effort with more complex interpolation methods. A suitable method for linear interpolation with nonuniform data is triangulating data and using linear barycentric interpolation.

The barycentric coordinate system describes a point's location in reference to a simplex. The barycentric coordinates have several useful properties. For example, the coordinates sum up to 1. The simplex is formed with Delaunay triangulation. Delaunay triangulation maximizes the minimum angle of the triangle iteratively. This method results in a good quality triangulation with fairly evenly sized simplices. One property that Delaunay has is that if a circle is drawn piercing vertices of any of the simplices, the circumcircle is empty of any vertices. The Delaunay triangulation is illustrated in Figure 5.1. The process of linear barycentric interpolation is described in more detail in [25]. In general, the interpolation follows the equation

$$x_{interp} = \sum_{i=1}^{n} a_i x_i, \tag{5.5}$$

where x_{interp} is the interpolated value, a_i is the value of i^{th} barycentric coordinate and x_i the value corresponding given coordinate. Variable i iterates from 1 to n, which is the number of vertices. In the two-dimensional case, the number of vertices is 3. This can

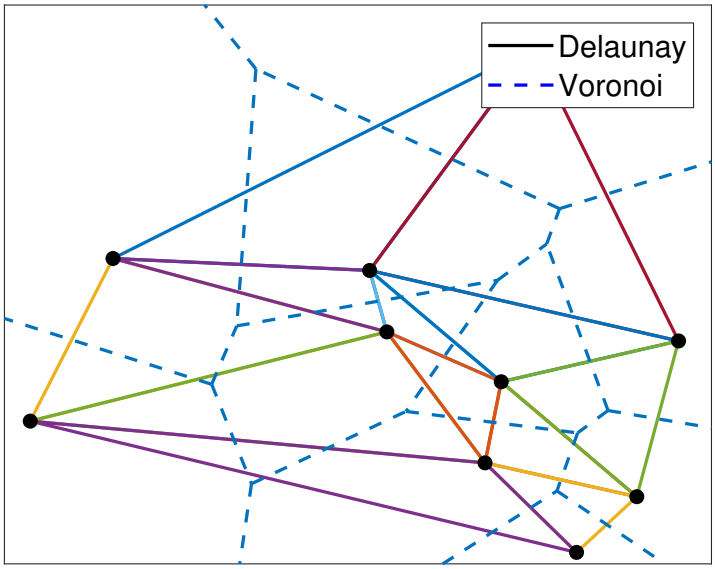

Figure 5.2. *Voronoi cells of 10 random data points*

be applied as an alternative method for finding the nearest neighbor as well. Voronoi diagram shares dual properties with Delaunay triangulation. The nearest neighbor of the point inside the Voronoi cell is the vertex inside the same cell. The process is described in [26]. This is illustrated in Figure 5.2, where the Voronoi diagram has been drawn over the previous Delaunay triangulation.

The same triangulation can be used also in cubic interpolation. There are many methods researched, such as bivariate piece-wise Clough–Tocher interpolation. This method creates local piece-wise polynomials, thus creating continuously differentiable interpolation for the triangulation area. The continuous first derivative is ensured by requiring linear perpendicular cross-boundary derivatives between the simplices. [27]

With larger matrices containing similar information, the process of interpolating values between the measurements can be done quite efficiently. In the case of nearest-neighbor interpolation, the search can be done only once, and the result can be used on all the layers of the matrices time domain using the indices returned by the search. The same applies to the linear interpolation. The triangulation is done first, and the same multipliers are then used with the data along the time domain. This makes the interpolation much faster. For triangulation, there are multiple efficient algorithms making this method ideal for the given problem.

5.2.2 Data transformation

The glass in the tempering furnace moves along the x-direction, as seen in Figure 5.3. Because of this, the transformation can be done with Equations 5.1 and 5.4. This reduces the complexity of the calculations and makes the whole algorithm faster.

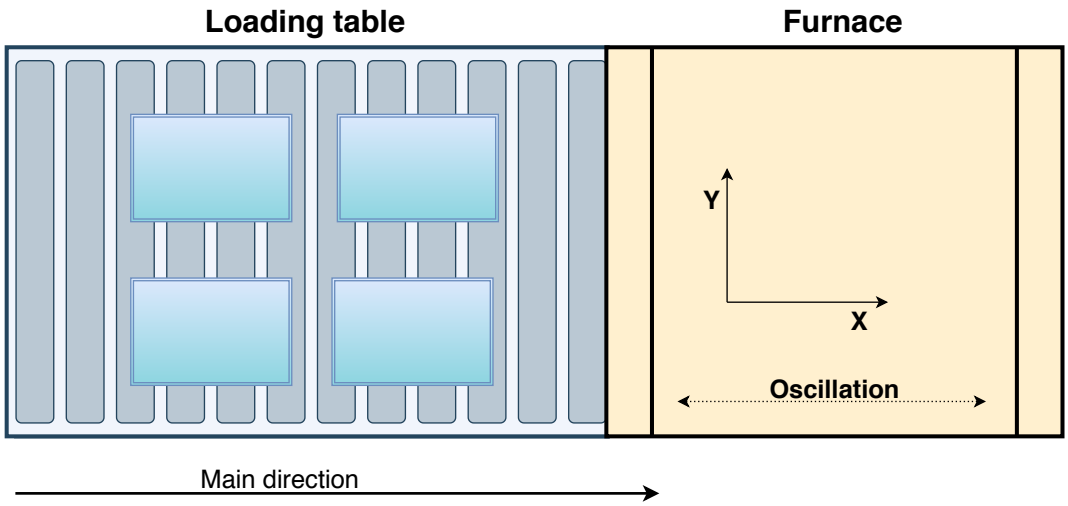

Figure 5.3. *Illustration of furnace coordinates*

Because the origin of time is chosen for each glass point separately to be the instant of furnace entrance for the point, the process of transforming coordinates has to be iterative. The transformation is done in two nested for-loops iterating first the data from the original matrix along time-dimension, and in the second loop along X-dimension. As the Y-dimensions stays the same, it can be done all at once.

Algorithm 1 Pseudo code of the conversion algorithm

```
1: for t = 0 : time_end do
2:     for x = 0 : x_end do
3:         t0 = time the coordinate entered the furnace
4:         x0 = Coordinate of the moving origin
5:         if t0 > t and x0+x <= Furnace length then
6:             glass_frame[x,:,t-t0] = furnace_reading[x+x0,:,t]
7:         end if
8:     end for
9: end for
```

As seen in Algorithm 1, the data is transformed in two nested for-loops with rather simple operations. The functions returning the time given coordinate has entered the furnace, and the origin of the new coordinates at a given time are omitted from the pseudo-code. These are simple and efficient to solve if the position curve of the origin is known. One way to improve the algorithm would be moving the procedure of copying data to the new matrix on line 6 outside of the loop, but here it is left inside to be more compact and easier to read.

If the movement of the origin is accelerated or decelerated while entering or exiting the furnace, the total time in the furnace depends on the point's location on the glass. Algorithm 1 is able to handle this situation. The time, when the glass has left the furnace at a given coordinate, can be determined from the transformed data.

6 FURNACE DATA ANALYSIS

The focus of this study is in the analysis of data converted to the glass coordinates. The data transformation can be done for a set of measurements, creating a data set S containing samples $s_m(X, Y, T)$ where X and Y refer to the position in the glass coordinates, T is time in glass coordinates, and subscript m is the index of measurement. From the furnace, four furnace/glass attributes were measured: the temperature above the glass,the temperature below the rollers, and the corresponding heater powers, respectively.

The furnace data were analyzed with two objectives in mind:

- estimation of the tempering result and
- detection of furnace anomalies.

In this Chapter, the PCA is used to describe the data of a single tempering instance, eg. tempering process of a batch of glass, and for a set of similar tempering instances. Tempering instances are called similar if the geometry of their layout is the same within the spatial resolution of the data analysis, and if the material properties of glasses in the batches are close enough, so that their thermodynamic behavior can be assumed identical up to the accuracy of the data analysis in this study.

The data was analyzed with PCA to achieve these goals. If the scope of analysis is in similar tempering instances, the differences in tempering results can be evaluated against one another with the same principal component loadings. The data in the following Sections is the temperature data measured at the top of the furnace and converted into the glass coordinates.

6.1 Principal component analysis for single tempering instance

The summary of data from a single tempering instance is presented in Figure 6.1 as the mean and standard deviation of temperature time series, computed over the X- and Y-locations. The sample mean is the factor that is subtracted from every time series in order to get the 0-centered data. This gives also the base in which the data is recreated from the PC scores. The standard deviation of the data is important in the sense of PCA because it affects the results of PCA. With the given standard deviation, the early parts

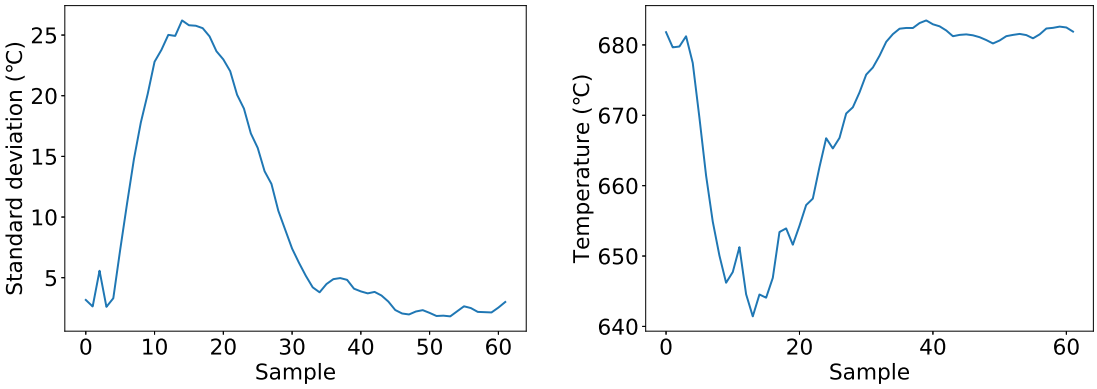

(a) *Standard deviation* ***(b)*** *Sample mean*

Figure 6.1. *Standard deviation and sample mean*

Component	1	2	3	4	5
Variance	8382.2	1647.3	163.3	112.3	82.3

Table 6.1. *Variances of the first five principal components of a single tempering instance*

of the time series are weighted more by the PC loadings. If the standard deviation were normalized, the weighting would be uniform. In this case, the data is not normalized as the interest in results lie in the early parts of the heating, where the anomalies in temperature are more critical for the final product.

Most of the variance in the data is on the first three principal components. Figure 6.2 shows that the first three principal components represent over 95 % of the variance. The next two principal components add 2.7 %. Figure 6.3 compares data reconstruction with one and five principal components to the original data at the location. Even the first principal component recreates the data and reduces the noise in the data.

The first five principal component loadings are shown in Figure 6.4. In the figure the first

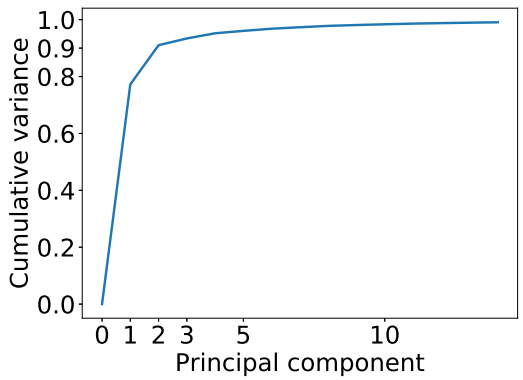

Figure 6.2. *Cumulative sum of the variance*

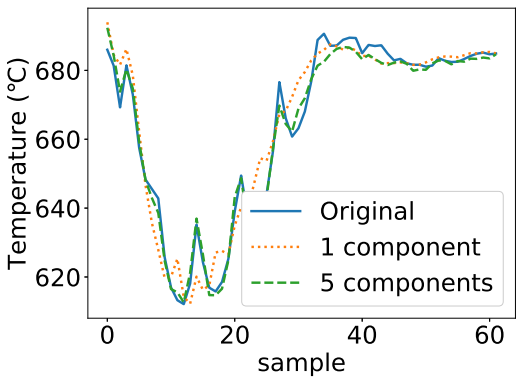

Figure 6.3. *Recreated estimation of the data*

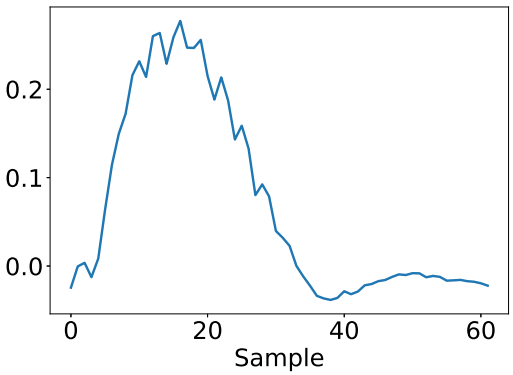

(a) *Principal component: 1*

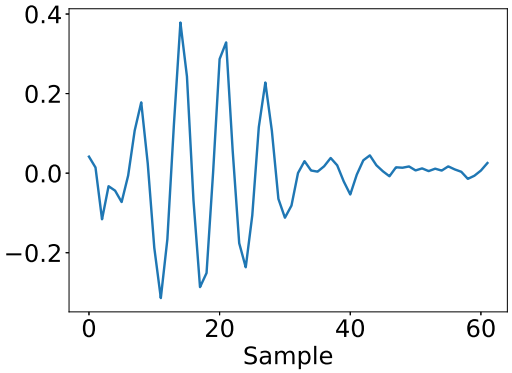

(b) *Principal component: 2*

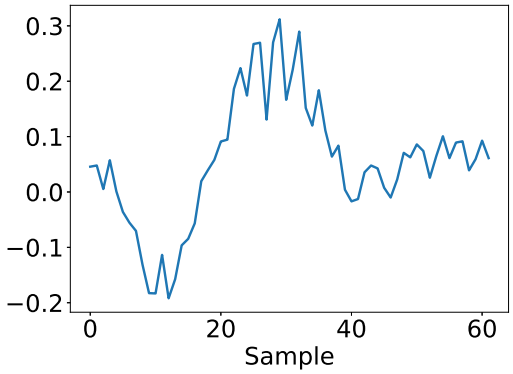

(c) *Principal component: 3*

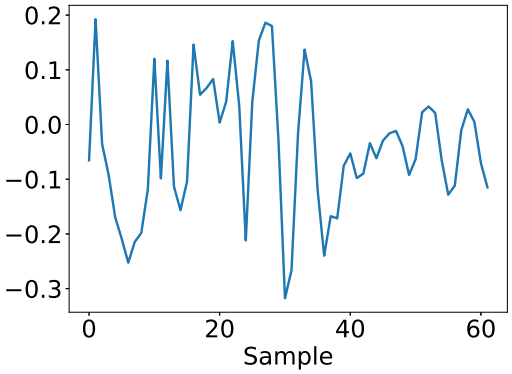

(d) *Principal component: 4*

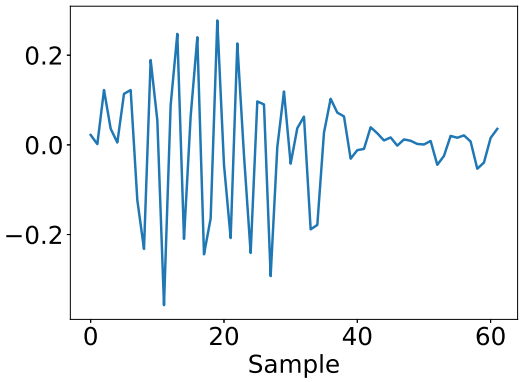

(e) *Principal component: 5*

Figure 6.4. *The first five principal component loadings of a single tempering instance*

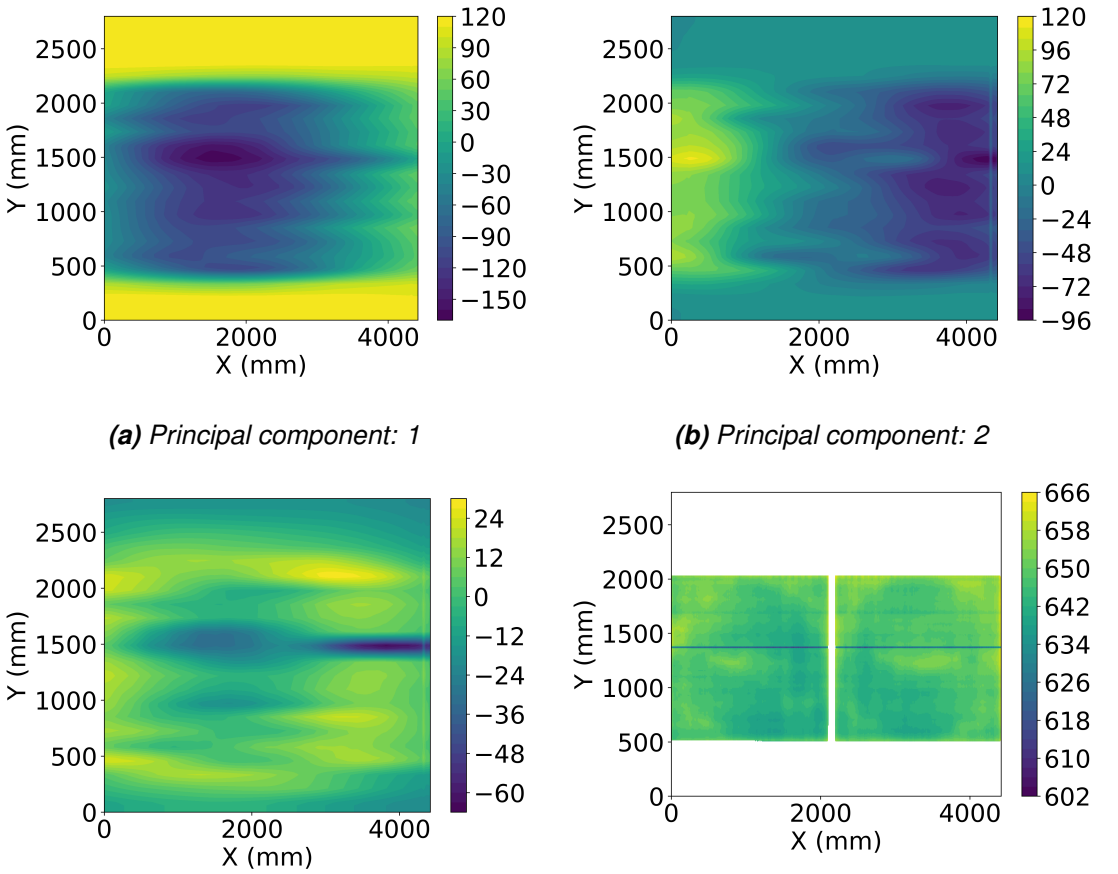

(a) *Principal component: 1*

(b) *Principal component: 2*

(c) *Principal component: 3*

(d) *Scanner image, where the horizontal line is a measurement error*

Figure 6.5. *First three principal component scores of a single tempering instance*

principal component resembles the shape of the averaged samples seen in Figure 6.1 **(b)** where the sample means are from the non-centered data. As the PCA scores are in descending order, the first PC loading defines the primary shape of the deviation from the average shape of time series.

As in the data matrix, the ordering of samples, indexed by location in glass coordinates, is irrelevant for PCA, the analysis does not imply any spatial structure. Therefore, any spatial structure arising in PCA scores means that the system under study, the tempering furnace, must be the cause for such structure. The first three principal component scores are illustrated in Figure 6.5, where the scores are presented in the X,Y -glass coordinates that correspond to the coordinates seen on the scanner image. The horizontal line in the scanner image is a measurement error caused by an object obstructing the line of sight of the scanner. In Figure 6.5 **(d)** is the scanner image of the tempered glass for illustration of the loading layout and its correspondence to the principal components. The first two principal components have a noticeable spatial structure that corresponds to the parts of the data where the glass has been. On the third principal component, the spatial structure is not that noticeable anymore, and the following components have decreasing structurality. At the same time the variation in scores starts to be more scattered along

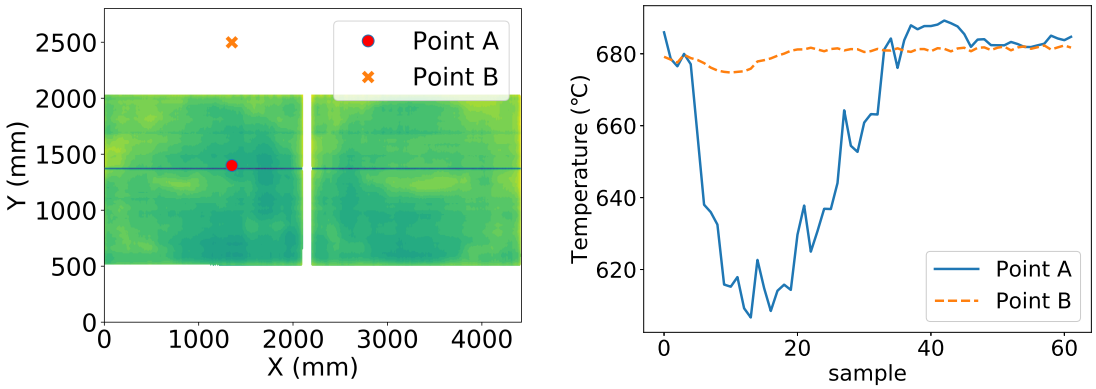

(a) *Positions of measurements* ***(b)*** *Measured temperatures*

Figure 6.6. *Temperatures above the glass and above unloaded rollers*

the X- and Y- dimensions. The main direction of the glass is from left to right, and the figures in glass coordinates throughout this work share the same orientation.

From the first two components, it can be noted how the variation in time series of the temperatures vary more along X-direction. The Subfigure 6.5 ***(a)*** describes the difference in components varying the most, and the second Subfigure 6.5 ***(b)*** describes respectively the difference in the component varying the second most in the data.

In Figure 6.1 ***(b)*** the drop in temperature is caused by cold glass entering the furnace and disturbing the temperature measurement. From the shape of the first principal component loading, it can be concluded that the temperature data has maximum variance in the shape of the temperature shock caused by the glass.

The first principal component score in Figure 6.5 has the highest values near the center of the glass layout and negative values in the area where there was not any glass. The positive values make the drop in temperature higher, whereas the negative values even out the temperature shock. This is illustrated in Figure 6.6, where the temperature above the empty rollers at point B does not drop almost at all while the temperature above the glass at point A drops below the mean temperatures seen in Figure 6.1.

The second PC loading contains an oscillating pattern, which can be explained by the oscillating movement of the glass. The second PC score values, illustrated in Figure 6.5, are positive on one end of the glass and negative on the other end of the glass. The negative sign turns the phase of the oscillation 180°. The same pattern occurs in the movement of the glass if, for example, the distance from glass leading edges to any fixed point is considered. The measurements from the opposite ends of the glass are illustrated in Figure 6.7. It can also be noted that the leading edge of the glass in the positive x-direction has a smaller temperature shock and final temperature. This part of the glass has been in the front half of the furnace where the glass has entered already significantly warmer after traveling through the furnace and therefore affecting less to the furnace temperature.

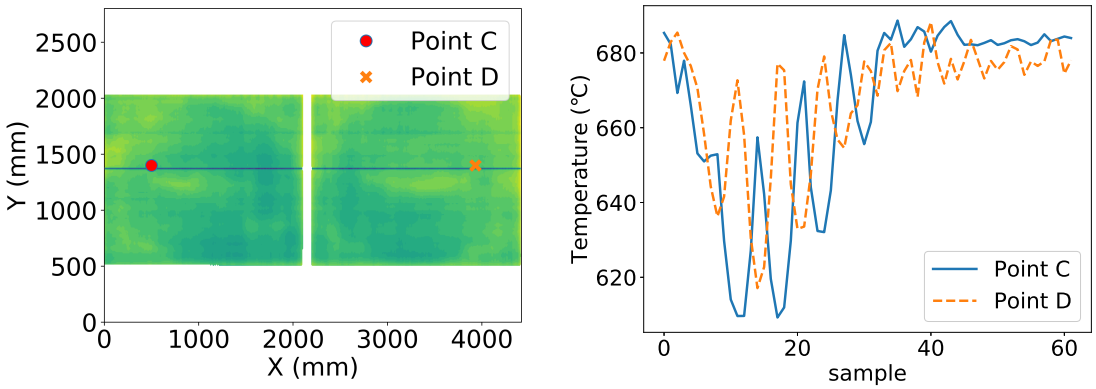

***(a)** Positions of measurements* ***(b)** Measured temperatures*

***Figure 6.7.** Temperatures at the different ends of the glass*

6.2 Principal component analysis for multiple similar tempering instance

The principal component analysis can be done for a set of tempering instances with similar layouts. This results in a set of data F, which contains PC scores $f_m(X, Y, r, k)$ where r is the index of tempering instance. The rest of the attributes follow the definition in Section 6.1.

The resulting transformation describes the deviation of the PC scores depending on the position of the measurement. This can be useful in the estimation of the different temperature time series in the furnace. The original sample s_m can be written as

$$s_m(X, Y, T, r) = \overline{s_m}(T) + \sum_k f_m(X, Y, r, k)\alpha_m(k, T) \tag{6.1}$$

where $\overline{s_m}(T)$ is the sample mean over X, Y and r at time T, $f_m(X, Y, r, k)$ is k $^{\text{th}}$ principal component score, and $\alpha_m(k, T)$ is the value of corresponding principal component loading at time T for measurement m.

The idea behind the study of multiple tempering instances is the similarity of layouts. This ensures that the changes in X- and Y -coordinates over different tempering instances are not caused by changes in loading layout. The similarity reduces the variables affecting the temperatures, such as changing the mass of the glass or different emissivity. However, it has to be noted that the glass panes are manually placed onto the loading table, and therefore small variation on the location of the glass panes is unavoidable.

The principal component scores can be averaged over the different tempering instances, thus creating an average model $\overline{F_m}(X, Y, k)$ of score along X- and Y-coordinates

$$\overline{F_m}(X, Y, k) = \frac{\sum_r f_m(X, Y, r, k)}{n}, \tag{6.2}$$

Component	1	2	3	4	5
Variance	6405.2	1143.2	196.9	150.2	70.4

Table 6.2. *Variances of the first five principal components of multiple tempering instances*

where n is the number of different tempering instances. These average scores can be used to create a model of variation in the tempering instances. The variation in data can be divided into groups based on the axis along which the variation occurs. The equation 6.1 can be written with mean scores

$$s_m(X,Y,T,r) = \overline{s_m}(T) + \sum_k \overline{F_m}(X,Y,k)\alpha_m(k,T) + \sum_k dF(X,Y,m,r,k)\alpha_m(k,T), \quad (6.3)$$

where dF is the deviation from $\overline{F_m}$

$$dF_m(r) = F_m(r) - \overline{F_m}. \quad (6.4)$$

In Equation 6.3, the second term accounts for average changes respect to time. The third term accounts for average changes respect to the location similar to all tempering instances, and the last term accounts for differences between tempering instances.

Similarly to Section 6.1, the principal components can be reduced to a few components satisfying requirements of total variance explained. With more samples, the number of components required can rise depending on the nature of the data. With 21 similar glass layouts, as used in the previous Section, the cumulative sum of the total variance was 96.1 % with five principal components shown in Figure 6.8. Although this is slightly less than the respective percentage with data from one tempering instance, most of the variance is still extracted by only a few principal components. However, some higher-order principal components may provide useful insight. For example, the seventh principal component score, corresponding only to 0.35 % of the overall variance, marked glass edges quite precisely, as seen in Figure 6.9. This indicates that the time series near the edges of the glass contain a unique component, not present in other parts of the measurement area. The shape of the seventh PC loading suggests that the temperature time series near the edges have a second minimum. The variances of the first five principal components are shown in Table 6.2.

The principal component scores averaged over tempering instances, $\overline{F_m}(X,Y,k)$ defined in Equation 6.2 are shown in Figure 6.10. The principal component scores are quite similar, as in the case of single tempering instance displayed in Figure 6.5. The main difference from the single tempering instance is that the average third principal component score appears to contain more noticeable spatial variation. The scanner image displayed in Figure 6.5 **(d)** is the average scanner image. However, it has to be noted that the images over tempering instances are not exactly comparable as the PC scores of single tempering instance are computed using different PC loadings.

The first and second principal component scores deviation from the average score is

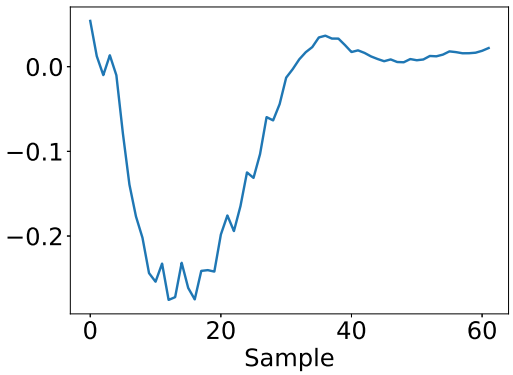

(a) *Principal component: 1*

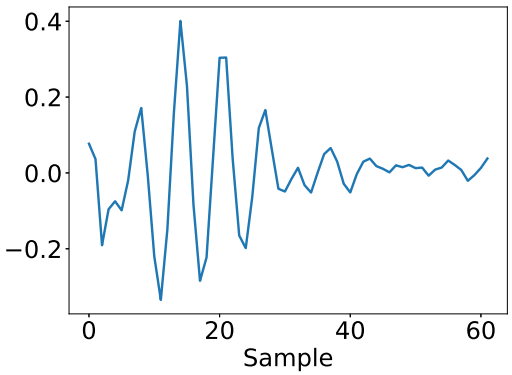

(b) *Principal component: 2*

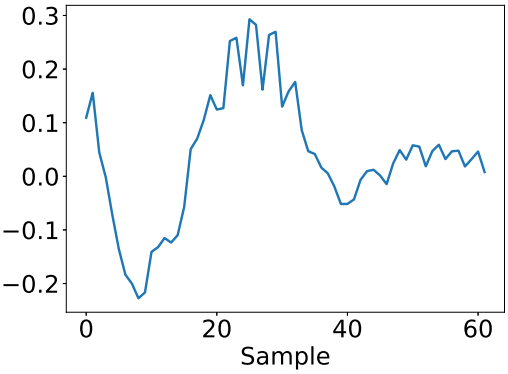

(c) *Principal component: 3*

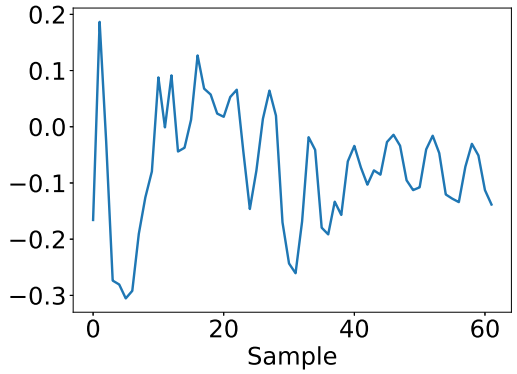

(d) *Principal component: 4*

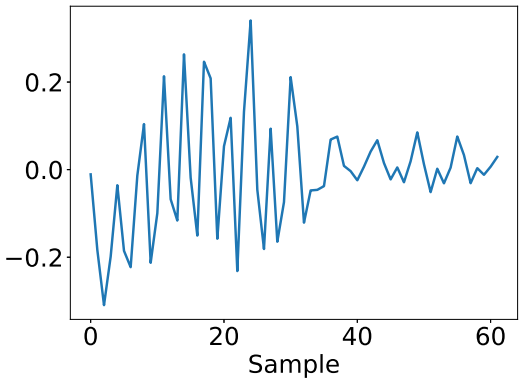

(e) *Principal component: 5*

Figure 6.8. *First five principal component loadings of a set of tempering instances*

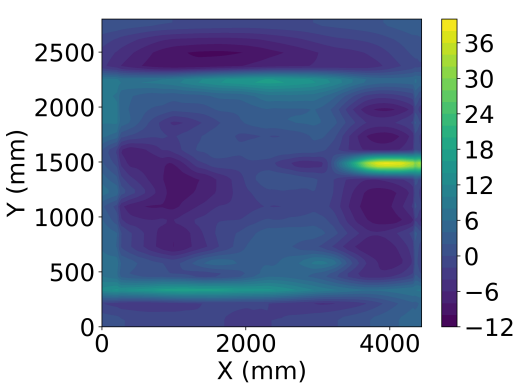

(a) Average seventh principal component score

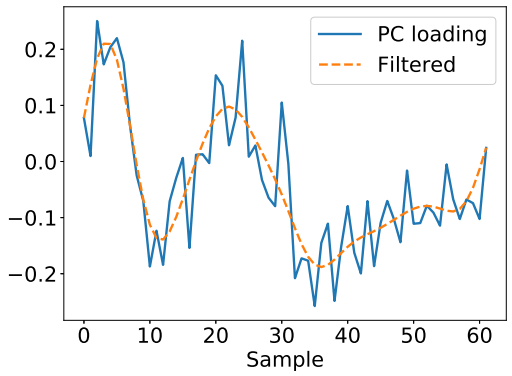

(b) Average seventh principal component loading and low pass filtered loading

Figure 6.9. *Principal component score and corresponding PC loading*

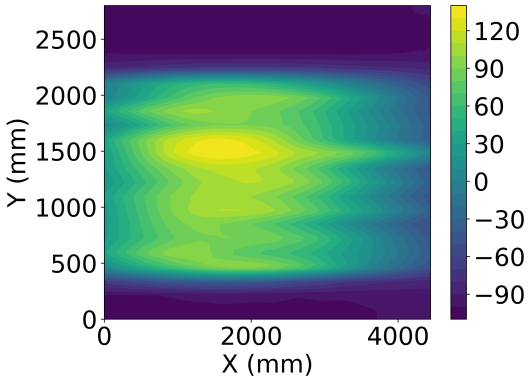

(a) Principal component: 1

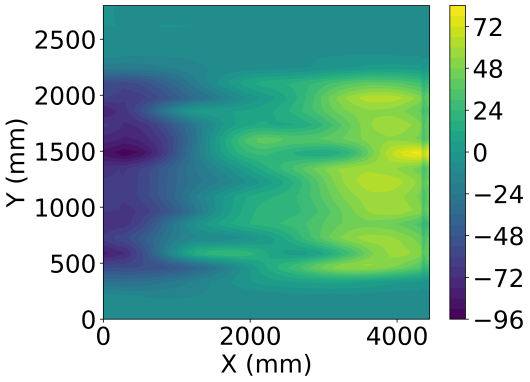

(b) Principal component: 2

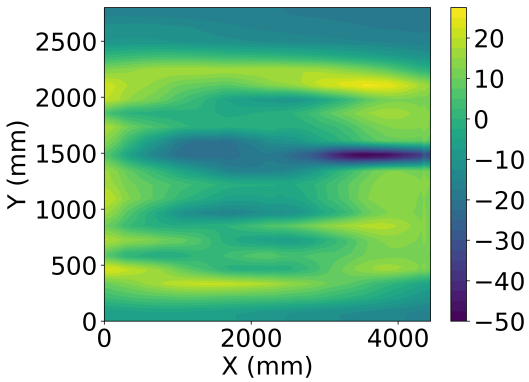

(c) Principal component: 3

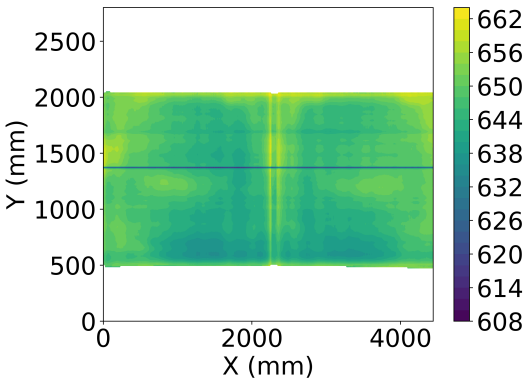

(d) Averaged scanner image

Figure 6.10. *Three average principal components scores of 21 tempering instances*

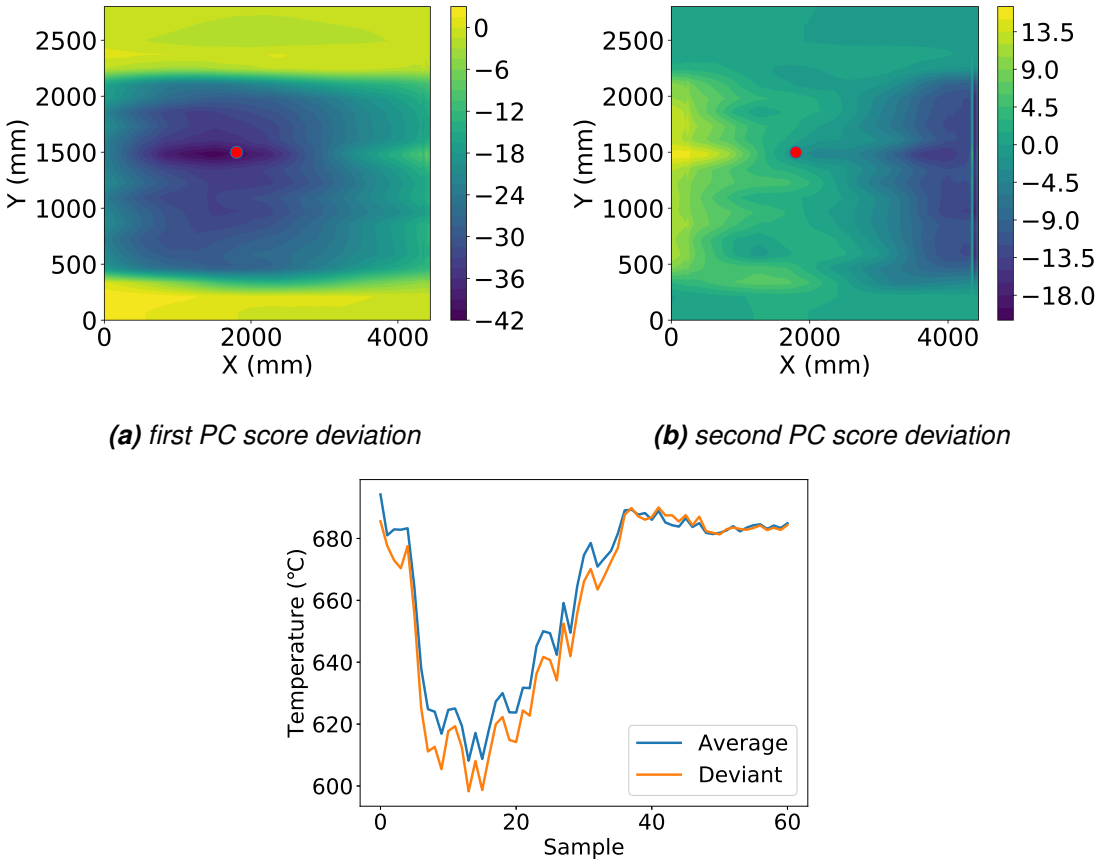

(a) *first PC score deviation*

(b) *second PC score deviation*

(c) *Average and deviant time series*

Figure 6.11. *Deviation from the average PC score*

illustrated in Figure 6.11. The deviations describe how much the scores of a single tempering instance differ from score average over all tempering instances. The tempering instance chosen for Figure 6.11 contained exceptional measurements among the tempering instances, and the lower temperatures are clearly visible in the lower figure of the average and deviant temperatures. The measurements were picked at point $X = 1800$ mm, $Y = 1500$ mm denoted by a red dot in Figures 6.11 **(a)** and **(b)** of PC score charts.

7 CASE: SET OF SIMILAR LAYOUTS

The methods of Section 6.2 were applied in a set of glass tempering instances with similar layouts. The focus on the experiment was in finding differences in the heating of the glass. The data set consisted of 81 similar tempering instances where an approximately 1.25 m by 4 m sized glass panes were treated.

The panes were tempered within approximately 18 hours. The recorded data included the temperatures above and below the glass, scanner images, and tempering recipes. The data of heaters' power was not available. An average scanner image of all tempering instances is shown in Figure 7.1. In the figure, the width has increased due to small deviations in the placement of the glass. This causes horizontal lines in the lower and upper edges of the glass.

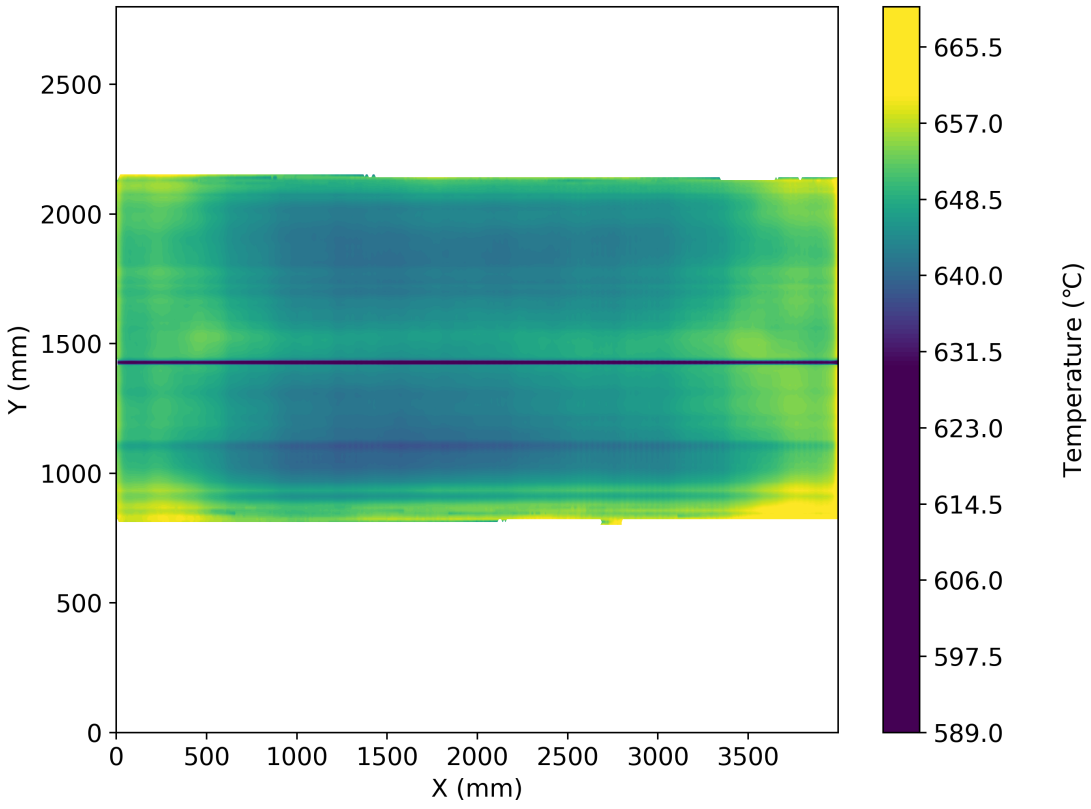

Figure 7.1. *Average scanner image*

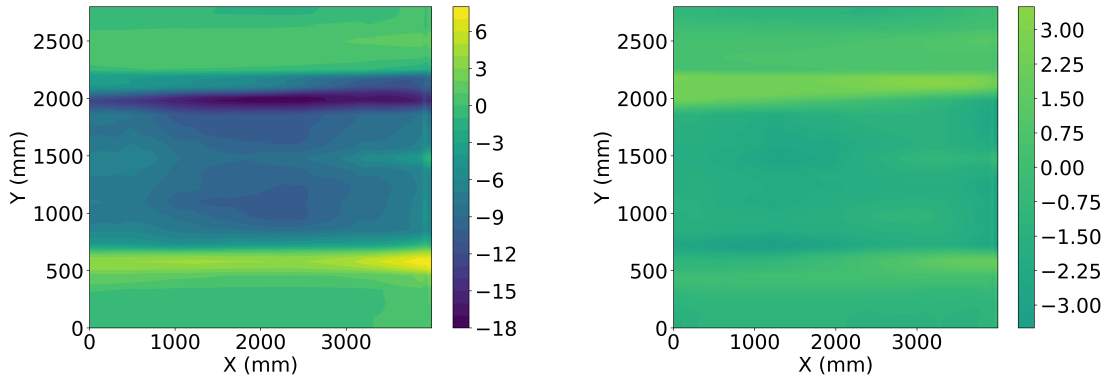

(a) *Deviant tempering instance's standard normal deviation*

(b) *Normal tempering instance's standard normal deviation*

Figure 7.2. *First principal component's score standard normal deviation*

7.1 Standard normal deviate of PCA scores

If the theory of SND from Section 4.5 is applied here, the equation 6.3 can be written as

$$\begin{aligned} s_m(X,Y,r,T) =& \overline{s_m}(T) + \sum_k \overline{F_m}(X,Y,k)\alpha_m(k,T) \\ &+ \sum_k \sigma_m(X,Y,k) SND_m(X,Y,k,r)\alpha_m(k,T) \end{aligned} \tag{7.1}$$

where $\sigma_m(X,Y,k)$ is the standard deviation of k^{th} principal component score at a location (X,Y) computed over the tempering instances and $SND_m(X,Y,k,r)$ the corresponding standard normal deviate of the score of the k^{th} principal component. The standard normal deviate describes the significance of the deviation at a given point. In Figure 7.2 is illustrated the difference between normal and deviant tempering instances' standard normal deviate of the first principal component.

SND enables detecting exceptional tempering instances and detecting within them parts of the glass that have exceptional temperature histories. Three methods were tested for detecting abnormal tempering instances automatically:

1. the proportion of locations with the absolute value of SND larger than 3,
2. the proportion of squared SND summed over locations with the absolute value of SND higher than 3 to the total sum of squared SND
3. mean of absolute SND values.

The detection scores from the methods listed above are illustrated correspondingly In Figure 7.3, where the mean values are normalized to the same scale [0, 1]. In the figure, the second method resulted in a good separation of the detection scores. The threshold value for the detection score could be set to 0.5. This result could be used for an automatic detection of deviant instances.

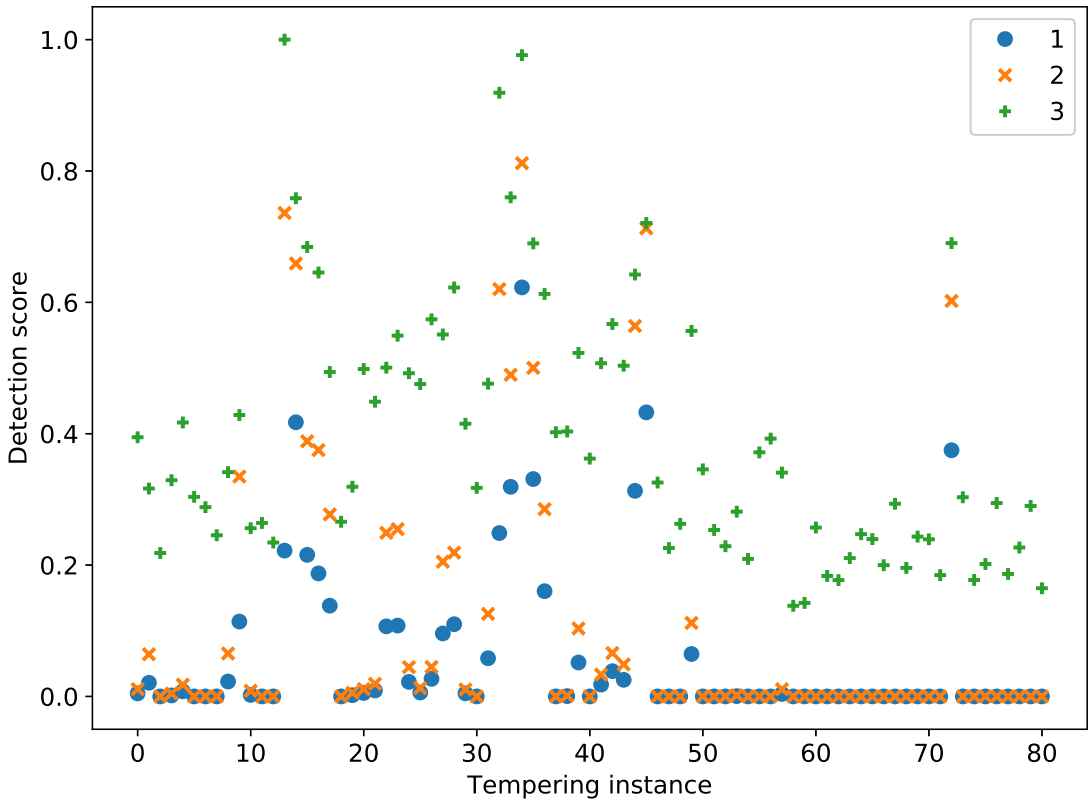

Figure 7.3. *Detection scores of the listed methods*

From the listed methods, the second method provided good results and was selected for the classification of deviant tempering instances.

In the second method, the SND values were summed first over X and Y

$$SND_m(k,r) = \sum_{X,Y} SND_m(X,Y,k,r) \tag{7.2}$$

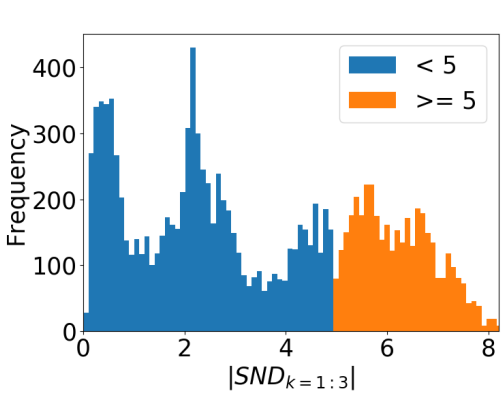

(a) *Histogram of absolute SND values.*

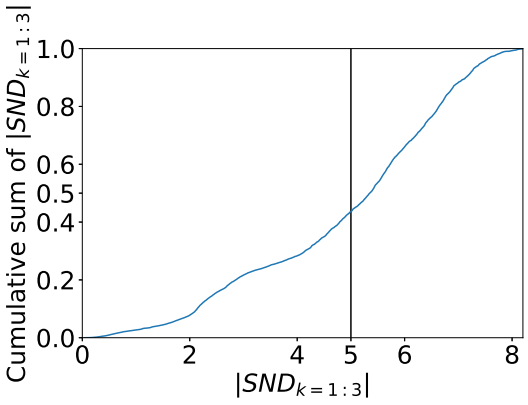

(b) *Cumulative sum of* $|\sum_{k=1}^{3} SND_k|$

Figure 7.4. *Elements of detection score*

Tempering	Top temperature	Bottom temperature
14	73.6	63.2
15	65.9	87.2
33	62.0	48.3
35	81.2	59.6
36	50.0	31.4
45	56.4	12.6
46	71.3	38.8
73	60.2	66.2

Table 7.1. *Detection scores: percentage of the total value of samples with sum of first 3 SND values greater than 5.*

and the result of the method, called detection score (DS_m) is

$$DS_m(r) = \frac{\sum_{k=1}^{n}(|SND_m(k,r)|H(|SND_m(k,r)| - a))}{\sum_{k=1}^{n}|SND_m(k,r)|}, \tag{7.3}$$

where a is a parameter for adjusting the sensitivity, H is Heaviside function, and n is the number of principal components used. For this set of data, a sensitivity parameter a was given value 5. The detection threshold was then determined manually by comparing detection scores and tempering results. The detection score in Equation 7.3 is illustrated in Figure 7.4, where the detection score is the proportion of cumulative sum above the value of a.

The measurements from above and below the glass were analyzed separately and PCA was done with measurement data from all tempering instances. 8 tempering instances resulted in DS value above the threshold for either measurement above or below the glass. The detection scores are illustrated in Table 7.1, and scores of all deviant instances are illustrated in Figure 7.5.

In Figure 7.5, the tempering instances 10–50 contain more variation than other tempering instances. During the end of the session, the tempering instances since 50$^{\text{th}}$ tempering instance are quite uniform, excluding 2 tempering instances near the end of the series.

7.2 Deviant instances

The average scanner image in Figure 7.1 illustrates how the glass is heated before the quenching. Both leading edges are warmer than the rest of the glass. There is a faint warmer horizontal line in the center of the glass. The final result of tempered glass with anaverage temperature profile has been likely straight glass with minimal optical imperfections.

The deviant instances contain two outliers, as some additional glass panes have been tempered along with the main piece. These are the 14$^{\text{th}}$ and 33$^{\text{rd}}$ tempering instances.

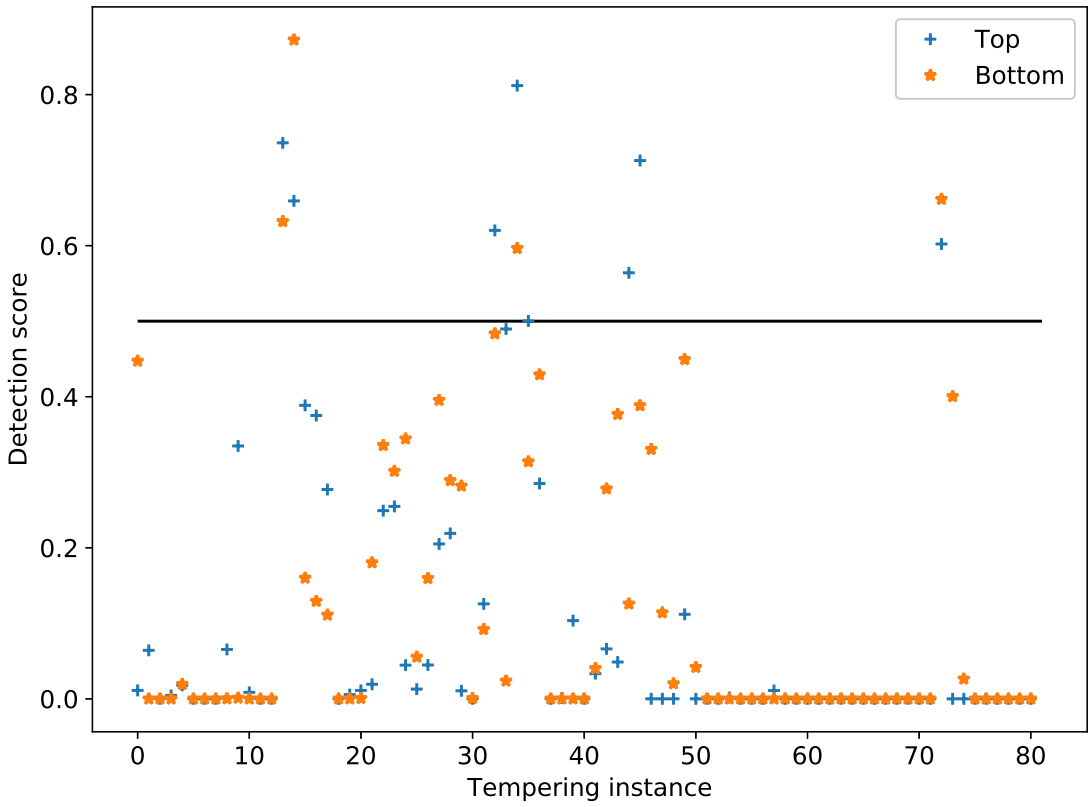

Figure 7.5. *Detection scores from the top and the bottom measurements of the 81 tempering instances using Eq. 7.3.*

In figure 7.6 is illustrated the 14^{th} tempering instance. The deviation from typical furnace temperature is explained in those cases by the increased mass of the extra panes.

The rest of the deviant tempering instances contain the same layout and, by a glance, seem identical to scanner images of normal tempering instances. Figure 7.7 illustrates a scanner image of a deviant tempering instance. In the figure, the horizontal line at the center of the glass is more noticeable than on the average scanner image.

The line is not the cause but a consequence of the deviant temperatures. The temperatures above and below the glass have been unbalanced, and the glass edges have lifted. This causes the glass to heat more from the center of the glass. Eventually the glass becomes flat again due to increased viscosity. The same effect is noticeable in all the deviant tempering instances, excluding the ones with the outliers. The mean scanner image of deviant tempering instances is shown in Figure 7.8. This deviation in temperatures could result in slightly bent glass or white haze in the center of the glass.

The differences in tempering instances can be examined by comparing the time series of the deviant tempering instances and normal tempering instances. The deviant tempering instances contain similar time series. The average deviation was calculated from deviant tempering instances for both measurements, and those were compared to the average time series of normal tempering instances at the same point. This is illustrated in Figure 7.9. Both measurements are lower than the corresponding average measurements.

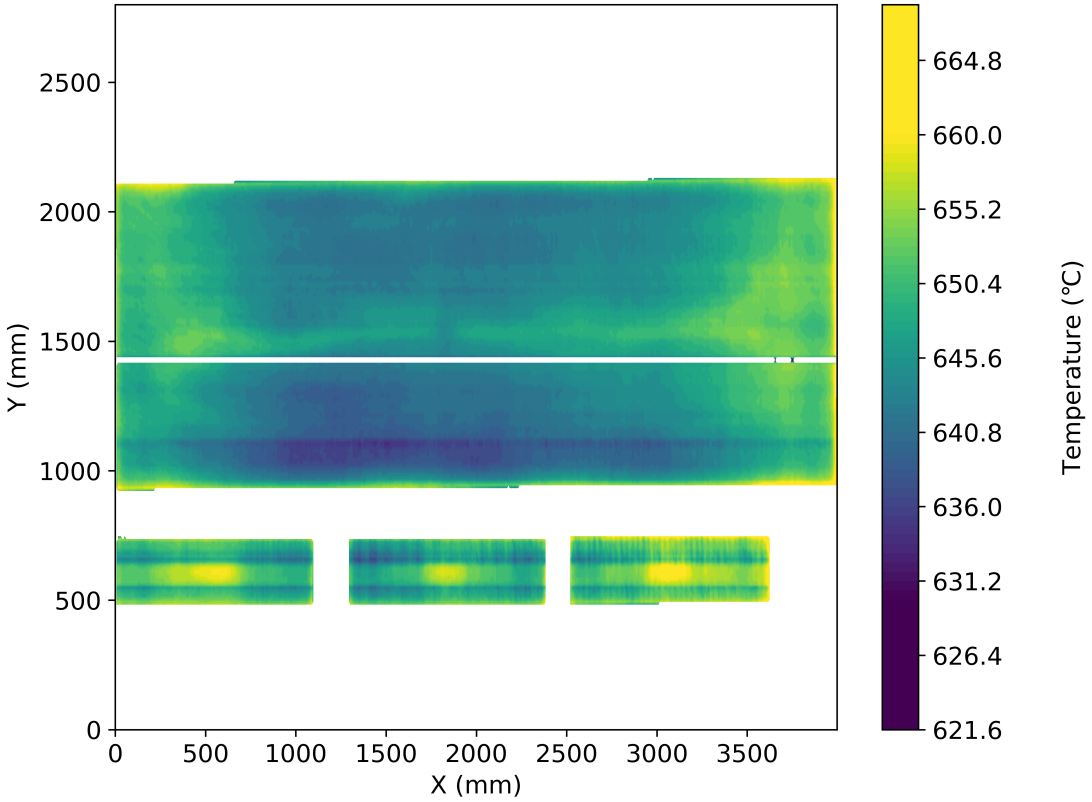

Figure 7.6. *14th tempering instance's scanner image*

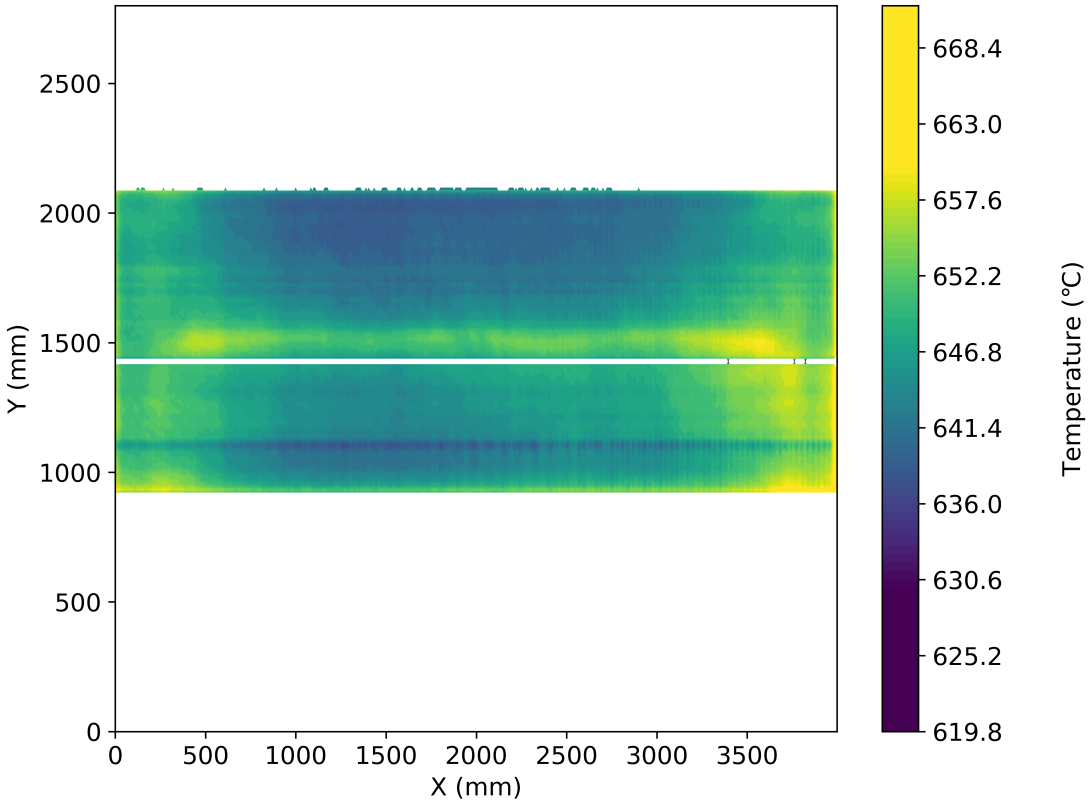

Figure 7.7. *73rd tempering instance's scanner image*

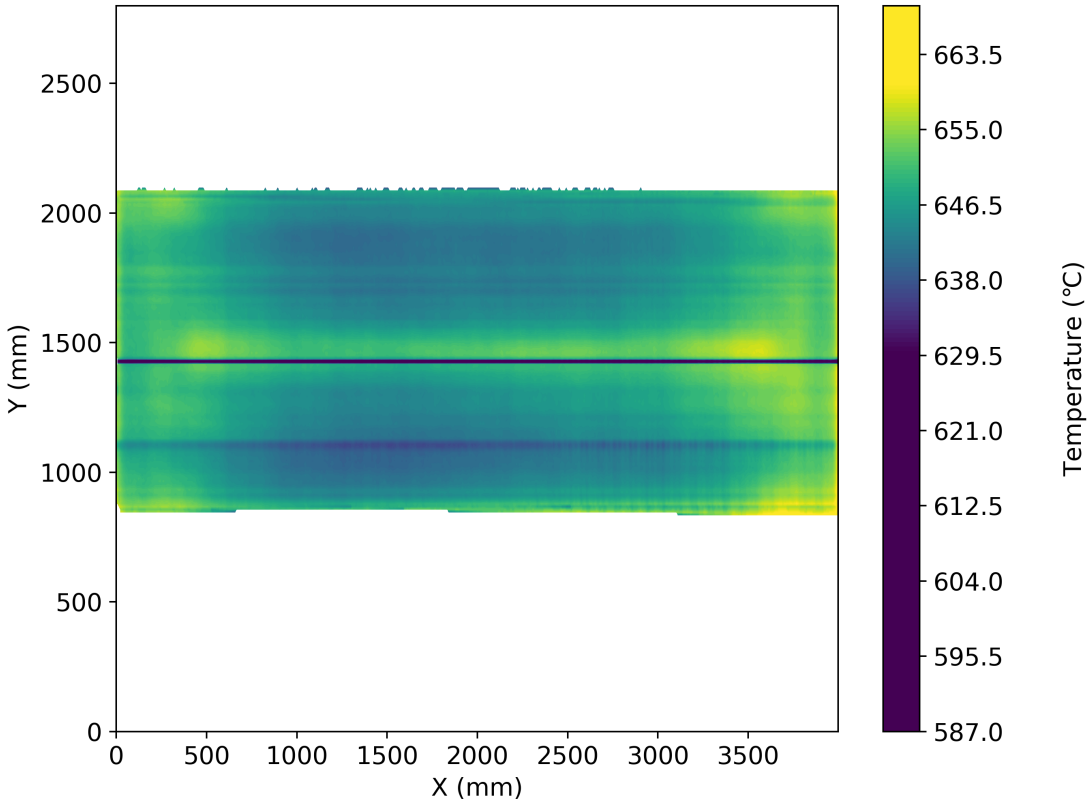

Figure 7.8. *Average scanner image of deviant tempering instances*

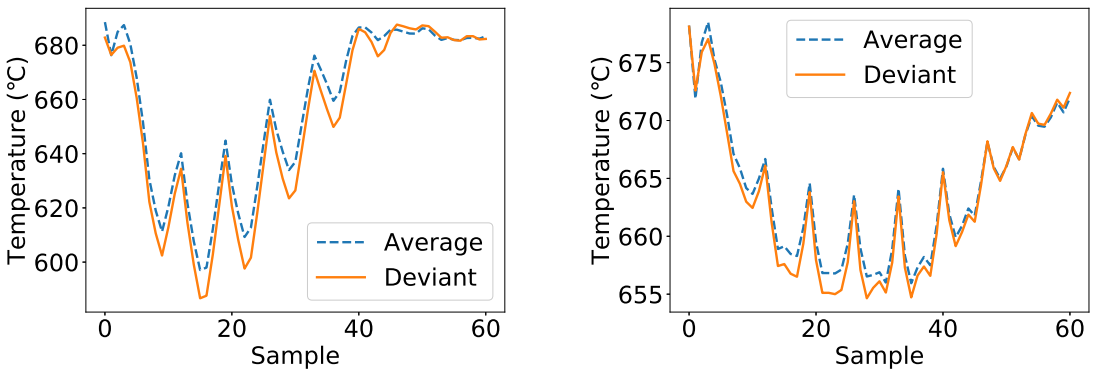

(a) *Top measurements* ***(b)*** *Bottom measurements*

Figure 7.9. *Average normal and deviant time series from point* $X = 2000, Y = 1650$

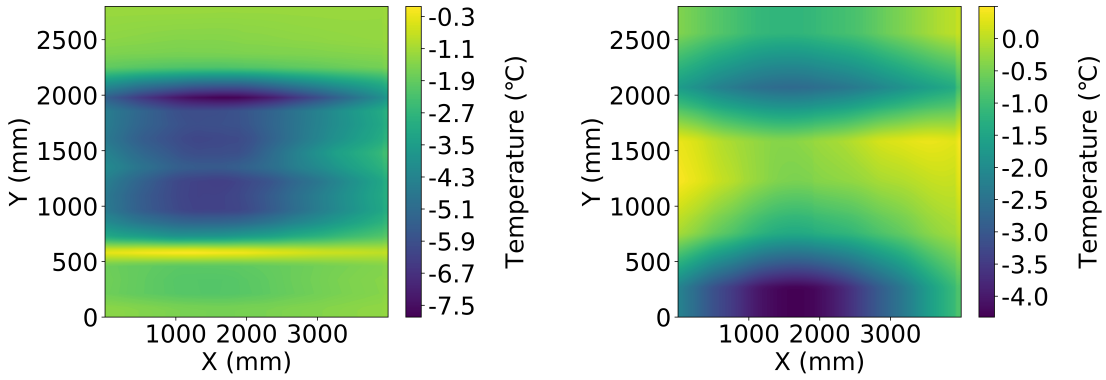

***(a)** Top average deviation* ***(b)** Bottom average deviation*

***Figure 7.10.** The average deviation of time series*

The same exploration for all points of measurement requires a lot of effort, and therefore, the method is simplified. The time series of deviant tempering instances are averaged over time and tempering instances. The same is done for the normal tempering instances, and the result is subtracted from the deviant mean. The result is called the average deviation, and it is illustrated for both measurements in figure 7.10.

7.3 Causes of deviation

In this Section, the causes of deviation are briefly discussed. As was noted at the beginning of this Chapter, the layout of the tempering instances is kept unchanged with two exceptions. The possible causes for deviations in tempering are, for example, changes in tempering recipe, the state of the furnace, or varying initial temperature of the glass.

The changes in the tempering recipe do not explain the deviation in tempering instances. Only one modification was made to the recipe. The heating time was decreased in the 34^{th} tempering instance by one second from 370 s to 369 s. The data does not contain any record of the state of the glass panes before the tempering process, so the affection of glass temperature cannot be investigated. It remains a subject worth researching in later studies.

The state of the furnace can be estimated roughly. No temperature data is logged while the furnace is idle, but the time between tempering instances can be evaluated from the data. The furnace state can also be evaluated by a logged parameter *Head load* that relates to the energy consumed in heating during the idle time. Table 7.2 is represents idle times and detection scores of each tempering instance. The numbers of deviant tempering instances are in bold numbers. It can be noted that the deviant tempering instances have rather long idle time before them. The exceptions for this are tempering instances 14 and 33 that had extra glass panes on the same tempering. The 36^{th} tempering instance has only 9 minutes idle time but is preceded by nearly 3 hours idle time. The 45^{th} tempering instance was preceded by a tempering process of a non-similar glass that was

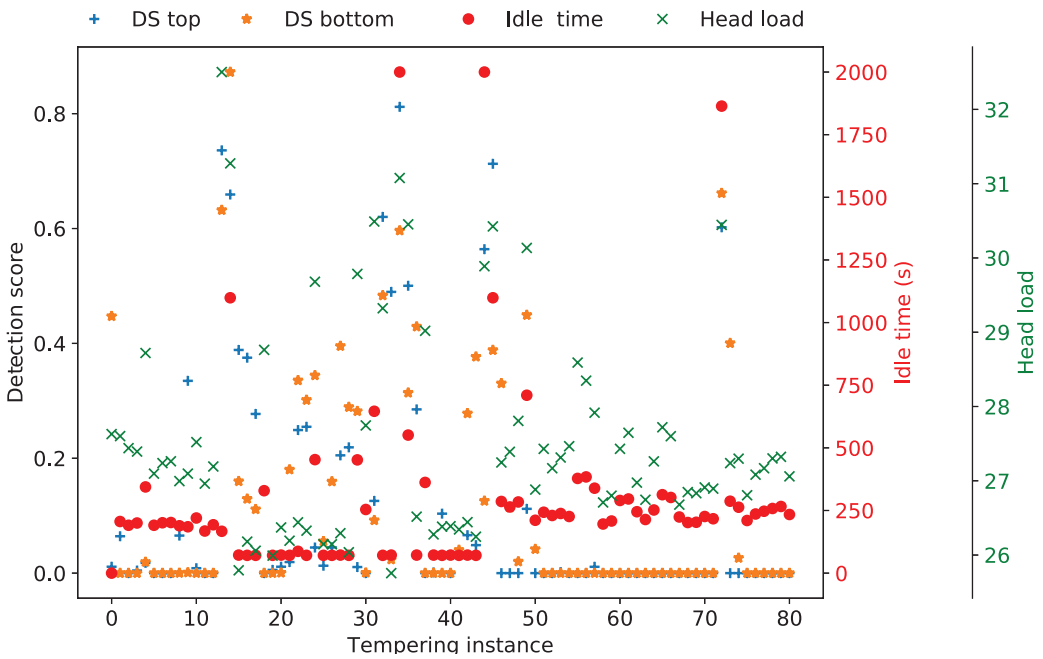

Figure 7.11. *Idle time and detection scores*

removed from the study.

The data from Table 7.2 is illustrated in Figure 7.11 as well as the head load. The idle time in the figure is limited to a maximum of 2000 seconds. The same conclusion, that the deviate tempering instances correlate with the idle time of the tempering furnace, can be made by inspecting the figure or the table. The figure illustrates perhaps more clearly the deviation in idle times during the tempering instances 15–45, where the detection scores seem to be varying more. Longer idle times seem to affect on 2–3 tempering instances following the pause.

The correlation of head load and idle time to detection scores is illustrated in Figure 7.12, where the detection score is on the x-axis and head load and idle time on the y-axis. A least-squares fit was made from the data. The correlation seems to explain some of the deviations but not explicitly, and there must be other variables that affect the deviation as well.

The results of this case are not directly generalizable for other cases, as there are many variables affecting the tempering results. For this combination of tempering recipe and tempered glass, the idle time seems to affect the results. This can be counteracted by adjusting the recipe or the furnace control during idle time.

7.4 Separate PCA for normal and deviant tempering instances

The principal component analysis was also done separately for normal and deviant tempering instances found in Chapter 7. The idea behind the separate analysis of deviant

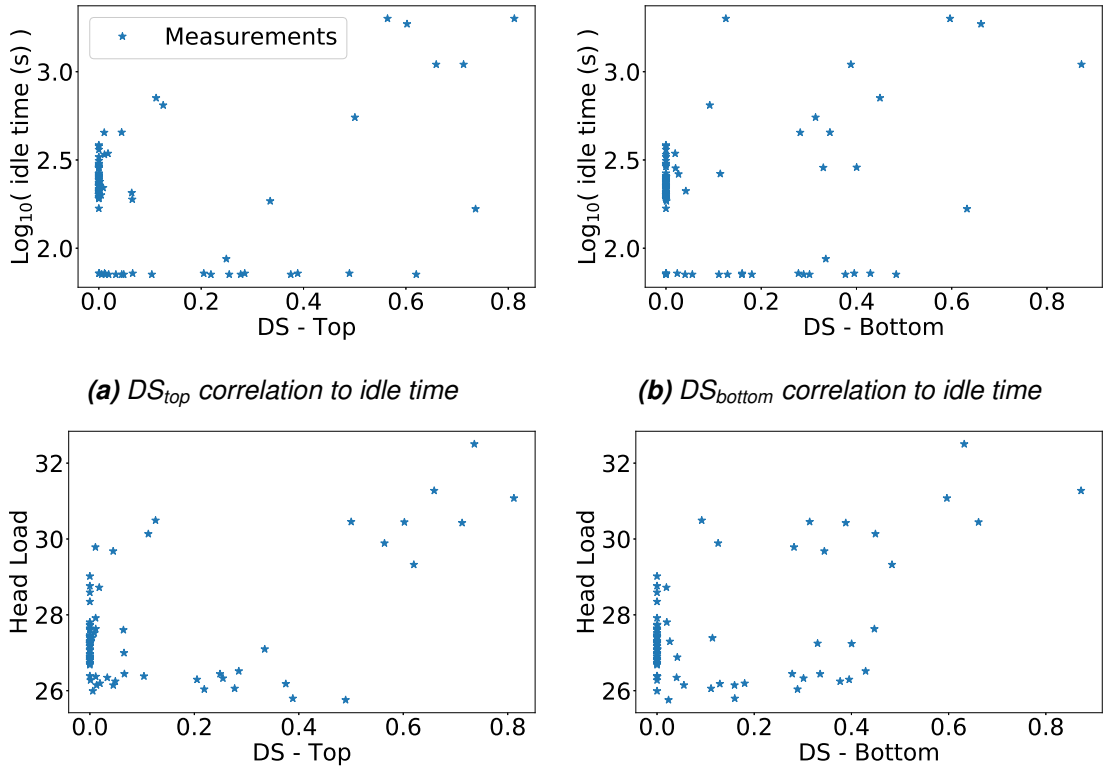

(a) *DS_{top} correlation to idle time*

(b) *DS_{bottom} correlation to idle time*

(c) *DS_{top} correlation to head load*

(d) *DS_{bottom} correlation to head load*

Figure 7.12. *Correlation of principal*

and normal tempering instances was to find out how the results change when data is analyzed with different principal components. Additionally, this could explain how the furnace behavior is changed in deviant tempering instances compared to normal tempering instances.

In order to keep results comparable, the same 0-centered data was used as in previous Sections, albeit the zero mean is not guaranteed for the subsets. The results with subsets of data seem quite similar even though the amount of data in the deviant set is significantly less than in the original set of data. The resulting principal components share the same structure as the original principal components; however, small variations can be noticed. In Figure 7.13, the first principal component loadings of data from normal and deviant tempering instances are illustrated. The data from deviant tempering instances produces a principal component loading that seems to return to average temperature slower than the corresponding principal component loading of the data from the normal tempering instances.

The detection scores have similar results as with all tempering instances. The detection scores produced by PC loadings from normal tempering instances are illustrated in Figure 7.14.

The same 7 tempering instances were detected as with the detection scores of the original PCA. As a result, it seems like this kind of deviations in the data will not affect that

Table 7.2. *Time between tempering instances*

Tempering	Idle time	DS top	DS bottom	Tempering	Idle time	DS top	DS bottom
1	0:00	1.1 %	44.7 %	41	1:12	0.0 %	0.0 %
2	3:26	6.4 %	0.0 %	42	1:11	3.3 %	4.0 %
3	3:11	0.0 %	0.0 %	43	1:12	6.6 %	27.8 %
4	3:20	0.4 %	0.0 %	44	1:11	4.9 %	37.7 %
5	5:44	1.8 %	1.9 %	**45**	35:27	56.4 %	12.6 %
6	3:11	0.0 %	0.0 %	**46**	18:19	71.3 %	38.8 %
7	3:21	0.0 %	0.0 %	47	4:46	0.0 %	33.0 %
8	3:22	0.0 %	0.0 %	48	4:24	0.0 %	11.4 %
9	3:09	6.5 %	0.0 %	49	4:44	0.0 %	2.0 %
10	3:05	33.5 %	0.1 %	50	11:50	11.2 %	44.9 %
11	3:40	0.9 %	0.0 %	51	3:31	0.0 %	4.2 %
12	2:48	0.0 %	0.0 %	52	4:03	0.0 %	0.0 %
13	3:13	0.0 %	0.0 %	53	3:50	0.0 %	0.0 %
14	2:47	73.6 %	63.2 %	54	3:58	0.2 %	0.0 %
15	18:19	65.9 %	87.2 %	55	3:46	0.0 %	0.0 %
16	1:12	38.9 %	16.0 %	56	6:18	0.0 %	0.0 %
17	1:11	37.5 %	12.9 %	57	6:24	0.0 %	0.0 %
18	1:11	27.7 %	11.1 %	58	5:39	1.1 %	0.0 %
19	5:29	0.0 %	0.0 %	59	3:16	0.0 %	0.0 %
20	1:11	0.6 %	0.0 %	60	3:28	0.0 %	0.0 %
21	1:12	1.1 %	0.1 %	61	4:50	0.0 %	0.0 %
22	1:11	1.9 %	18.0 %	62	4:56	0.0 %	0.0 %
23	1:27	24.9 %	33.6 %	63	4:05	0.0 %	0.0 %
24	1:11	25.5 %	30.1 %	64	3:34	0.0 %	0.0 %
25	7:33	4.5 %	34.4 %	65	4:12	0.0 %	0.0 %
26	1:11	1.3 %	5.5 %	66	5:13	0.0 %	0.0 %
27	1:11	4.5 %	15.9 %	67	5:02	0.0 %	0.0 %
28	1:12	20.5 %	39.5 %	68	3:44	0.0 %	0.0 %
29	1:11	21.9 %	28.9 %	69	3:22	0.0 %	0.0 %
30	7:32	1.1 %	28.2 %	70	3:23	0.0 %	0.0 %
31	4:14	0.0 %	0.1 %	71	3:46	0.0 %	0.0 %
32	10:46	12.6 %	9.2 %	72	3:37	0.0 %	0.0 %
33	1:11	62.0 %	48.3 %	**73**	31:04	60.2 %	66.2 %
34	1:12	49.0 %	2.4 %	74	4:47	0.0 %	40.0 %
35	175:9	81.2 %	59.6 %	75	4:23	0.0 %	2.6 %
36	9:10	50.0 %	31.4 %	76	3:30	0.0 %	0.0 %
37	1:12	28.5 %	42.9 %	77	3:56	0.0 %	0.0 %
38	6:02	0.0 %	0.0 %	78	4:07	0.0 %	0.0 %
39	1:12	0.1 %	0.0 %	79	4:18	0.0 %	0.0 %
40	1:11	10.4 %	0.0 %	80	4:26	0.0 %	0.0 %
				81	3:54	0.0 %	0.0 %

much to the results of PCA. The principal component analysis is strongly related to the covariance matrix of the data. Any bias in the data does not affect to the principal component loadings as long as the mean has been removed in calculation of the covariance.

7.5 Calculating detection scores without outliers

Another approach for refining the results of the detection score is the removal of outliers from the data. The standard deviation in Equation 4.32 affects directly to the detection score, and the outliers increase the standard deviation. The outliers, therefore, reduce the sensitivity of the detection score.

Figure 7.15 illustrates the detection scores calculated, excluding the outliers from the standard deviation. As predicted, the sensitivity of the detection score has increased. The values have not changed equally, and for example, the 34^{th} tempering instance's detec-

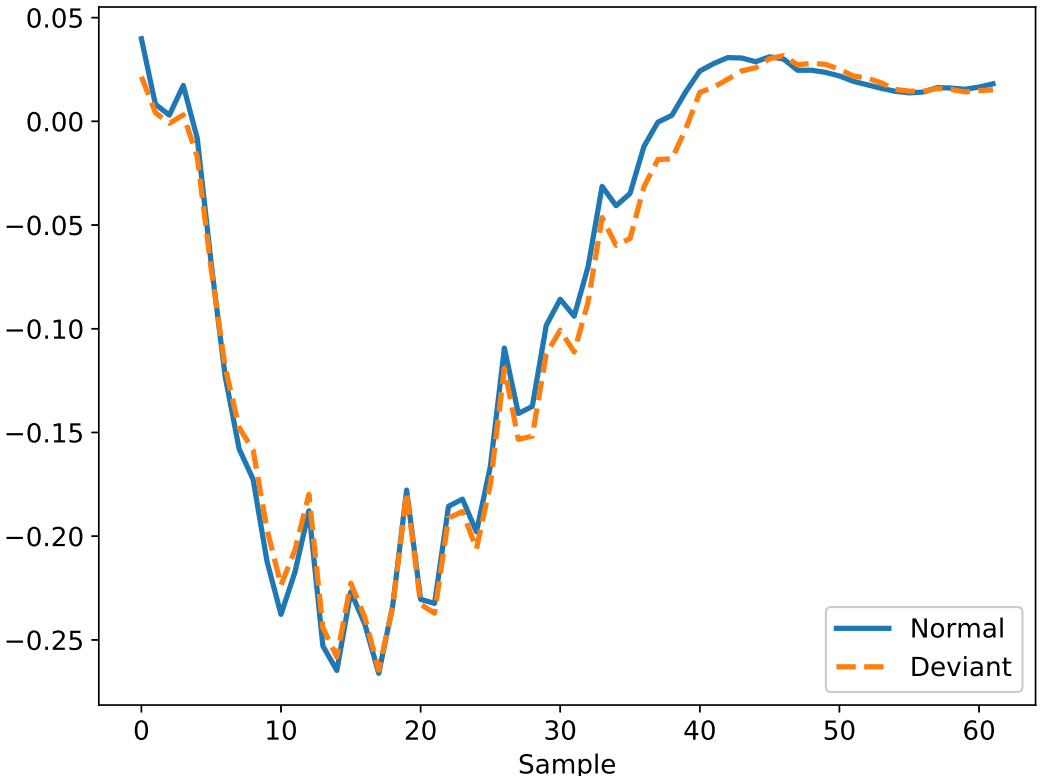

Figure 7.13. *First principal component loading of data from deviant and normal tempering instances.*

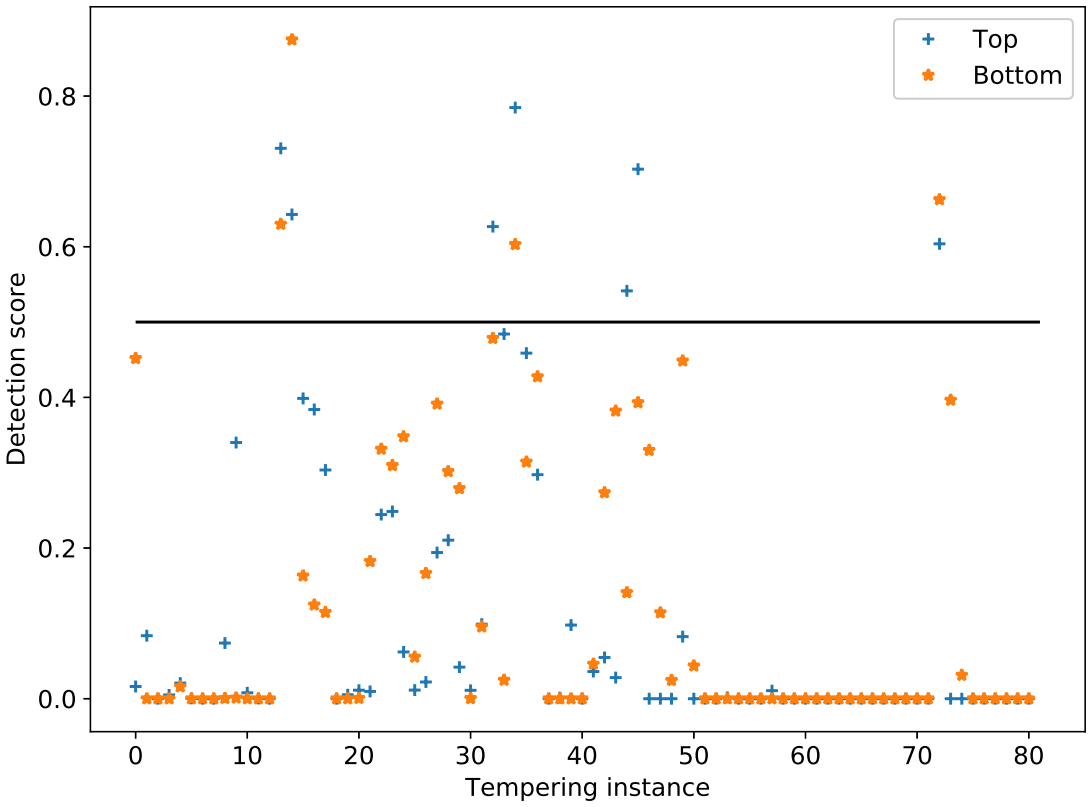

Figure 7.14. *Detection score from PCA with only normal tempering instances*

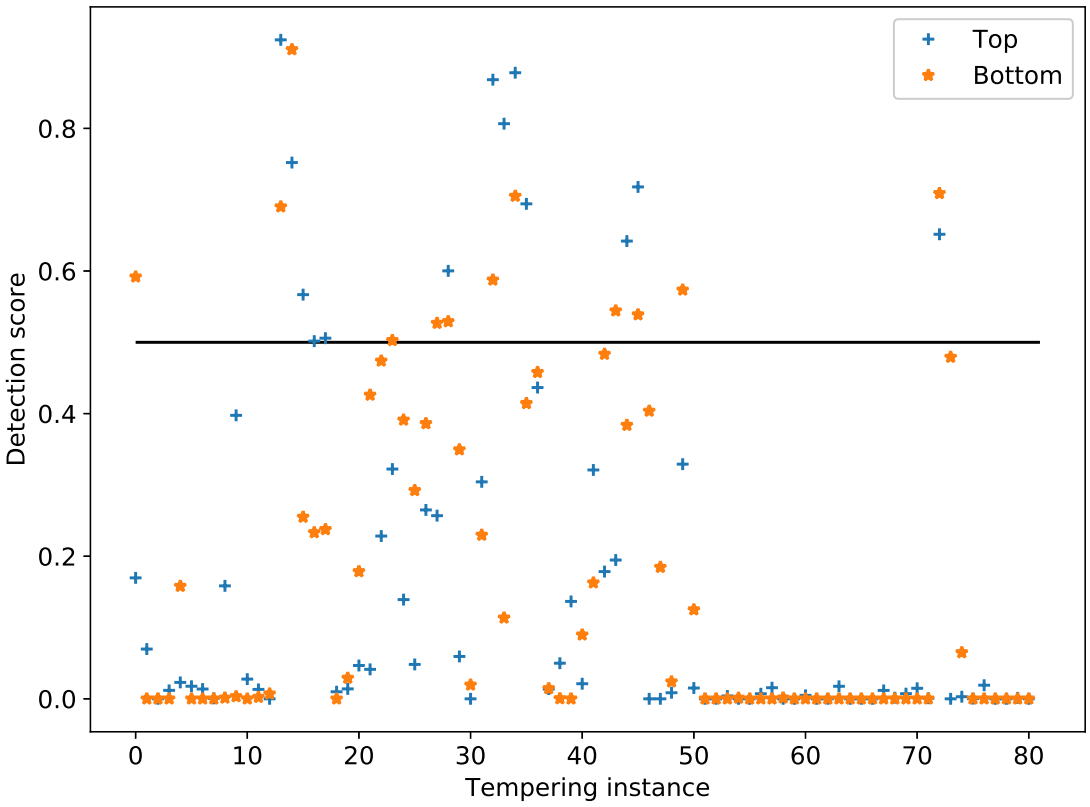

Figure 7.15. *Detection scores when outliers are not included in standard deviation*

tion score has risen significantly. Increasing the threshold of detection score could reduce the number of detected samples, or the sensitivity parameter a could be increased.

The detection scores were updated by increasing parameter a from value 5.0 to 5.5 and the results are illustrated in Figure 7.16. In the figure, the tempering instances with detection score above the threshold of 0.5 remain the same with the exception of 34th tempering instance. The 34th tempering instance is approximately one minute after the tempering of a layout with extra glass panes, and the effects of the different layout are probably still affecting during that tempering instance.

The detection of deviant instances is more accurate with increased sensitivity gained from the better estimate of the standard deviation of the deviates of scores. An option to mitigate the effect of deviant instances is the removal of deviant instances from the calculation of standard deviation after a primary detection. A more sophisticated solution for this problem could be an outlier robust estimate of standard deviation.

Robust statistics allow estimating the standard deviation of the PCA score deviates. An example of an outlier robust estimate of the standard deviation is the median absolute deviation (MAD) described in [28] or the interquartile range (IQR). The robust estimation of scale is widely studied, and more about it can be read from [29].

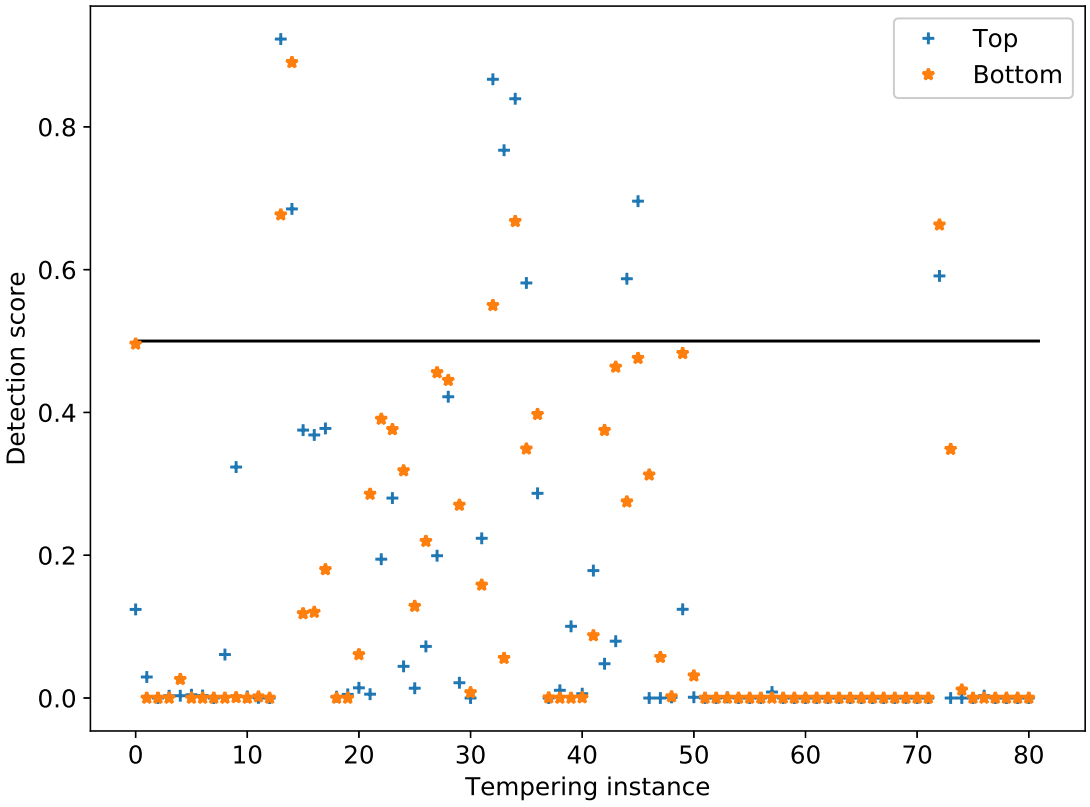

Figure 7.16. *detection scores with parameter a increased from 5.0 to 5.5*

8 CONCLUSION

The production of tempered glass faces multiple factors that have to be taken into account in order to achieve high-quality tempered glass. Small variations in glass temperature or uneven heating of the glass can result in the breakage of the glass during the process or unsatisfactory tempering results. The focus of this thesis was on the transformation of the measurements from stationary furnace coordinates into moving glass coordinates and the evaluation of the resulting data using PCA in order to estimate tempering results. An additional goal was automatic detection of unsuccessful or deviant tempering instances.

The conversion of furnace data from stationary frame to the moving glass frame was successful. The algorithm was able to interpolate and extrapolate data from the furnace and convert data from hundreds of tempering instances automatically and efficiently. The converted furnace measurements were then evaluated in glass coordinates. The data was analyzed with principal component analysis. In the analysis, a set of data from multiple tempering instances was used in order to produce a model of typical heating data. The model was then compared to each tempering instance in order to distinguish deviations from the average tempering instance.

The first few PC scores produced a clear spatial structure, which indicates that the measured time series contained a spatial structure as well and that the structure correlated with the layout of the tempered glass panes. With the PCA, it was possible to compress time series into a few PC scores while extracting most of the variance of the data. The PC scores were analyzed and used to detect deviant tempering instances.

For a set of 81 consecutive tempering instances that contained similar layouts, the PC scores were analyzed. From the PC scores, 8 deviant tempering instances were found by calculation of the proportion of absolute standard normal deviates of the PC scores above a certain threshold. The number of detected deviant tempering instances increased to 9 when the standard deviation of the PC scores was recalculated, excluding the outliers.

The results showed that the method was able to detect deviant tempering instances, and the scanner image of the glasses temperature profile verified the detections. The idle time before tempering and the result of tempering were also found out to be correlating with tempering recipe used in the test set.

For further analysis, an outlier robust method of calculating the standard deviation should be researched. This could improve the detection sensitivity and make it possible to create an automatic method of detecting deviant tempering instances. The findings of this study

could also be verified with more research, and the correlation between the idle time and results of tempering could be researched more.

REFERENCES

[1] A. O. Uusitalo. *Float Glass Innovation in the Flat Glass Industry*. Springer International Publishing, 2014. ISBN: 3-319-06828-8.

[2] M. Haldimann, A. Luible, and M. Overend. IABSE, 2008. ISBN: 978-3-85748-119-2. URL: https://app.knovel.com/hotlink/toc/id:kpSUGSED09/structural-use-glass/structural-use-glass.

[3] M. Rantala. *Heat Transfer Phenomena in Float Glass Heat Treatment Processes*. Kone- ja tuotantotekniikan laitos - Department of Mechanical Engineering and Industrial Systems ; Rakennetun ympäristön tiedekunta - Faculty of Built Environment, Tampere University of Technology, 2015, 135.

[4] L. F. Francis, B. J. H. Stadler, and C. C. Roberts. *Materials Processing - A Unified Approach to Processing of Metals, Ceramics and Polymers*. Elsevier, 2016. ISBN: 978-0-12-385132-1. URL: https://app.knovel.com/hotlink/toc/id:kpMPAUAPME/materials-processing/materials-processing.

[5] Jones, A. C., Hitchman, and M. L. *Chemical Vapour Deposition - Precursors, Processes and Applications*. Royal Society of Chemistry, 2009. ISBN: 978-0-85404-465-8. URL: https://app.knovel.com/hotlink/toc/id:kpCVDPPA04/chemical-vapour-deposition/chemical-vapour-deposition.

[6] Bishop and C. A. *Vacuum Deposition onto Webs, Films, and Foils*. William Andrew Publishing, 2007. ISBN: 978-0-8155-1535-7. URL: https://app.knovel.com/hotlink/toc/id:kpVDWFF001/vacuum-deposition-onto-2/vacuum-deposition-onto-2.

[7] J. Barr. *The Glass Tempering Handbook—Understanding the Glass Tempering Process*. Self Published, 2015. URL: http://www.lambertgtservices.co.uk/book/TheGlassTemperingHandbook.pdf.

[8] A. Aronen. *Modelling of Deformations and Stresses in Glass Tempering*. English. Tampere University of Technology. Publication. Tampere University of Technology, Apr. 2012. ISBN: 978-952-15-2799-9.

[9] M. Illguth, C. Schuler, and Ö. Bucak. The effect of optical anisotropies on building glass façades and its measurement methods. In: *Frontiers of Architectural Research* 35 (Apr. 2015), pp. 119–126. DOI: 10.1016/j.foar.2015.01.004.

[10] E. Hecht and A. Zając. *Optics*. World student series. Addison-Wesley Pub. Co., 1974. URL: https://books.google.fi/books?id=eLruAAAAMAAJ.

[11] R. Decourcelle, G. Kaminski, and F. Serruys. Controlling Anisotropy. In: *Glass Performance Days 2017* (2017), pp. 157–160. URL: https://www.gpd.fi/GPD2017_proceedings_book/GPD2017_conference_book.pdf.

[12] A. Aronen and R. Karvinen. Explanation for edge bending of glass in tempering furnace. In: *Proceedings of Glass Performance Days* (2009). Acceessed: 27.9.2019, pp. 575–579. URL: https://apps.glassglobal.com/gpd/downloads/Tempering-Aronen.pdf.

[13] R. Färm. *Taking the mystery out of anisotropy*. Accessed: 26.9.2019. 2019. URL: https://www.glastory.net/taking-the-mystery-out-of-anisotropy.

[14] K. P. F.R.S. LIII. On lines and planes of closest fit to systems of points in space. In: *The London, Edinburgh, and Dublin Philosophical Magazine and Journal of Science* 2.11 (1901), 559–572. DOI: 10.1080/14786440109462720. eprint: https://doi.org/10.1080/14786440109462720. URL: https://doi.org/10.1080/14786440109462720.

[15] H. Abdi and L. J. Williams. Principal component analysis. In: *Wiley Interdisciplinary Reviews: Computational Statistics* 2.4 (2010), 433–459. DOI: 10.1002/wics.101. eprint: https://onlinelibrary.wiley.com/doi/pdf/10.1002/wics.101. URL: https://onlinelibrary.wiley.com/doi/abs/10.1002/wics.101.

[16] I. T. Jolliffe. *Principal Component Analysis*. Springer Series in Statistics. New York: Springer-Verlag, 2002. ISBN: 0-387-95442-2. DOI: 10.1007/b98835. URL: http://www.springer.com/statistics/statistical+theory+and+methods/book/978-0-387-95442-4.

[17] J. Gentle. *Matrix Algebra: Theory, Computations, and Applications in Statistics*. Springer Texts in Statistics. Springer New York, 2007. ISBN: 9780387708737. DOI: https://doi.org/10.1007/978-0-387-70873-7.

[18] P. R. Peres-Neto, D. A. Jackson, and K. M. Somers. How many principal components? stopping rules for determining the number of non-trivial axes revisited. In: *Computational Statistics & Data Analysis* 49.4 (2005), 974–997. ISSN: 0167-9473. DOI: https://doi.org/10.1016/j.csda.2004.06.015. URL: http://www.sciencedirect.com/science/article/pii/S0167947304002014.

[19] X. Li, W. Lam, and M. Tam. New automatic incident detection algorithm based on traffic data collected for journey time estimation. In: *Journal of Transportation Engineering* 139.8 (2013). cited By 4, 840–847. DOI: 10.1061/(ASCE)TE.1943-5436.0000566.

[20] C. Mak and H. Fan. Transferability of expressway incident detection algorithms to Singapore and Melbourne. In: *Journal of Transportation Engineering* 131.2 (2005). cited By 9, 101–111. DOI: 10.1061/(ASCE)0733-947X(2005)131:2(101).

[21] K. Balke, C. Dudek, and C. Mountain. Using probe-measured travel times to detect major freeway incidents in Houston, Texas. In: *Transportation Research Record* 1554 (1997). cited By 5, 213–220. URL: https://www.scopus.com/inward/record.uri?eid=2-s2.0-5344242473&partnerID=40&md5=5089a30e39bbb748f50b537ce476adcb.

[22] Y.-M. Wu and C.-c. Chen. Seismic reversal pattern for the 1999 Chi-Chi, Taiwan, MW 7.6 earthquake. In: *Tectonophysics* 429.1-2 (2007). cited By 33, 125–132. DOI: 10.1016/j.tecto.2006.09.015.

[23] S. Öztürk. A statistical assessment of current seismic quiescence along the North Anatolian fault zone: Earthquake precursors. In: *Austrian Journal of Earth Sciences* 106.2 (2013). cited By 5, 4–17. URL: https://www.scopus.com/inward/record.uri?eid=2-s2.0-84891601812&partnerID=40&md5=65a955785443ae77f1a222108420eb63.

[24] S. Maneewongvatana and D. M. Mount. On the Efficiency of Nearest Neighbor Searching with Data Clustered in Lower Dimensions. In: *Computational Science — ICCS 2001*. Ed. by V. N. Alexandrov, J. J. Dongarra, B. A. Juliano, R. S. Renner, and C. J. K. Tan. Berlin, Heidelberg: Springer Berlin Heidelberg, 2001, pp. 842–851. ISBN: 978-3-540-45545-5.

[25] M. S. Floater and J. Kosinka. Barycentric Interpolation and Mappings on Smooth Convex Domains. In: *Proceedings of the 14th ACM Symposium on Solid and Physical Modeling*. SPM '10. Haifa, Israel: ACM, 2010, pp. 111–116. ISBN: 978-1-60558-984-8. DOI: 10.1145/1839778.1839794. URL: http://doi.acm.org/10.1145/1839778.1839794.

[26] F. Aurenhammer, R. Klein, and D.-T. Lee. *Voronoi diagrams and delaunay triangulations*. English. 2013. ISBN: 9789814447638.

[27] P. Alfeld. A Trivariate Clough-tocher Scheme for Tetrahedral Data. In: *Comput. Aided Geom. Des.* 1.2 (Nov. 1984), 169–181. ISSN: 0167-8396. DOI: 10.1016/0167-8396(84)90029-3. URL: http://dx.doi.org/10.1016/0167-8396(84)90029-3.

[28] T. Pham-Gia and T. Hung. The mean and median absolute deviations. In: *Mathematical and Computer Modelling* 34.7-8 (2001). cited By 84, 921–936. DOI: 10.1016/S0895-7177(01)00109-1. URL: https://www.scopus.com/inward/record.uri?eid=2-s2.0-0034815860&doi=10.1016%2fS0895-7177%2801%2900109-1&partnerID=40&md5=9391fc612c1539623e85133e50392f17.

[29] P. Huber. *Robust Statistics*. Wiley, 1981. ISBN: 9780471418054. DOI: 10.1002/0471725250.ch8.